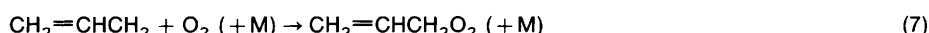
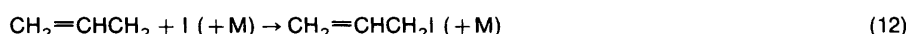
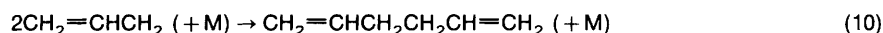


## Kinetics and Product Study of the Self-reactions of Allyl and Allyl Peroxy Radicals at 296 K

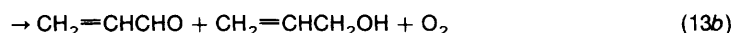
Michael E. Jenkin,\* Timothy P. Murrells, Stephen J. Shalliker† and Garry D. Hayman  
AEA Environment and Energy, Building 551, Harwell Laboratory, Didcot, Oxon OX11 0RA, UK

The laser flash photolysis technique, coupled with UV absorption spectroscopy, has been used to investigate the UV spectra and kinetics of reactions of the allyl radical ( $\text{CH}_2=\text{CHCH}_2$ ) and the allyl peroxy radical ( $\text{CH}_2=\text{CHCH}_2\text{O}_2$ ) at 296 K and total pressures near atmospheric.  $\text{CH}_2=\text{CHCH}_2$  radicals were generated by the 193 nm photolysis of hexa-1,5-diene- $\text{N}_2$  mixtures, or the 248 nm photolysis of allyl iodide- $\text{N}_2$  mixtures. The 193 nm photolysis of hexa-1,5-diene- $\text{O}_2$ - $\text{N}_2$  mixtures was used to generate  $\text{CH}_2=\text{CHCH}_2\text{O}_2$ . The low resolution spectrum of  $\text{CH}_2=\text{CHCH}_2$  was characterised in the range 210–232.5 nm. The absolute absorption cross-section near the maximum,  $\sigma$  (220 nm) =  $(5.8 \pm 0.8) \times 10^{-17} \text{ cm}^2 \text{ molecule}^{-1}$ , calibrated relative to the loss of allyl iodide, is in good agreement with the single published determination. The observed time dependence of  $\text{CH}_2=\text{CHCH}_2$  in the various chemical systems allowed measurement of rate coefficients for the following reactions



The parameters obtained were  $k_{10} = (3.0 \pm 0.5) \times 10^{-11}$ ,  $k_{12} = (1.6 \pm 0.6) \times 10^{-10}$ , and  $k_7 = (6 \pm 2) \times 10^{-13} \text{ cm}^3 \text{ molecule}^{-1} \text{ s}^{-1}$ .

The UV absorption spectrum of  $\text{CH}_2=\text{CHCH}_2\text{O}_2$ , characterised in the wavelength range 210–300 nm, is typical of an organic peroxy radical, with a peak cross-section of  $(6.2 \pm 0.9) \times 10^{-18} \text{ cm}^2 \text{ molecule}^{-1}$  at 235 nm.  $\text{CH}_2=\text{CHCH}_2\text{O}_2$  displayed second-order kinetic behaviour indicative of its removal *via* the self-reaction:



The observed rate coefficient,  $k_{13\text{obs}} = (1.1 \pm 0.2) \times 10^{-12} \text{ cm}^3 \text{ molecule}^{-1} \text{ s}^{-1}$ , is greater than the elementary coefficient,  $k_{13}$ , owing to secondary removal of  $\text{CH}_2=\text{CHCH}_2\text{O}_2$ . The observed and elementary coefficients are related by the expression  $k_{13\text{obs}} = (1 + \alpha_{13})k_{13}$ , where  $\alpha_{13} = k_{13a}/k_{13}$ . Associated long pathlength Fourier transform infrared (FTIR) measurements of the products of the 253.7 nm initiated photo-oxidation of allyl iodide, allowed the product channels of reaction (13) to be identified and quantified, and a value of  $\alpha_{13} = 0.61 \pm 0.07$  was determined, leading to  $k_{13} = (6.8 \pm 1.3) \times 10^{-13} \text{ cm}^3 \text{ molecule}^{-1} \text{ s}^{-1}$ .

The kinetic and mechanistic data obtained for  $\text{CH}_2=\text{CHCH}_2\text{O}_2$ , and those measured previously in this laboratory for  $\text{HOCH}_2\text{CH}_2\text{O}_2$ , are used to infer average rate coefficients for peroxy radicals ( $\text{RO}_2$ ) formed in the OH-initiated oxidation of isoprene. A simple box model of the planetary boundary layer is used to demonstrate the potential impact of elevated concentrations of isoprene on ambient levels of OH,  $\text{HO}_2$ ,  $\text{RO}_2$ ,  $\text{O}_3$  and  $\text{NO}_x$ .

The role played by organic peroxy radicals ( $\text{RO}_2$ ) in the tropospheric oxidation of volatile organic compounds is well documented.<sup>1–4</sup> The peroxy radicals, which are formed mainly from the attack of OH on the parent organic molecule, may have several competing reactions available, depending on the prevailing ambient conditions. If  $\text{NO}_x$  levels are high enough, the propagating reaction of  $\text{RO}_2$  with NO tends to dominate, leading ultimately to the production of  $\text{O}_3$  and other photo-oxidants which may contribute to reduced air quality:

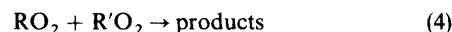
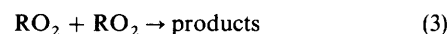


At lower levels of  $\text{NO}_x$ , other reactions become significant for  $\text{RO}_2$ , in particular the terminating reaction with  $\text{HO}_2$ , which inhibits  $\text{O}_3$  production by competing with reaction (1):



Generally, the ambient concentrations of  $\text{HO}_2$  are much greater than those of the  $\text{RO}_2$  radicals themselves. Under

certain circumstances, however, this is not the case, and the self- and cross-reactions of  $\text{RO}_2$  are also significant:



Measurements of elevated concentrations of reactive non-methane hydrocarbons of biogenic origin (especially terpenes) in the planetary boundary layer above remote forested regions<sup>5–10</sup> indicate that they will provide the major local sink for OH. Consequently, the production rates and concentrations of a range of complex  $\text{RO}_2$  radicals derived from the terpenes will be high (*i.e.* comparable with  $\text{HO}_2$ ) over widespread regions and, depending on the level of  $\text{NO}_x$ , it is possible for reactions of types (1)–(4) to be simultaneously competitive.

Although a great deal of progress has been made in recent years in defining structure–reactivity relationships for both kinetics and branching ratios of reactions of  $\text{RO}_2$  radicals,<sup>3,4</sup> there are currently insufficient data to predict the likely reactivity of the complex  $\text{RO}_2$  radicals formed from the oxidation of terpenes. The OH radical initiated oxidation of the simplest and most abundant (hemi-) terpene, isoprene, leads to

† Present address: School of Chemistry, University of Birmingham, Edgbaston, Birmingham B15 2TT, UK.

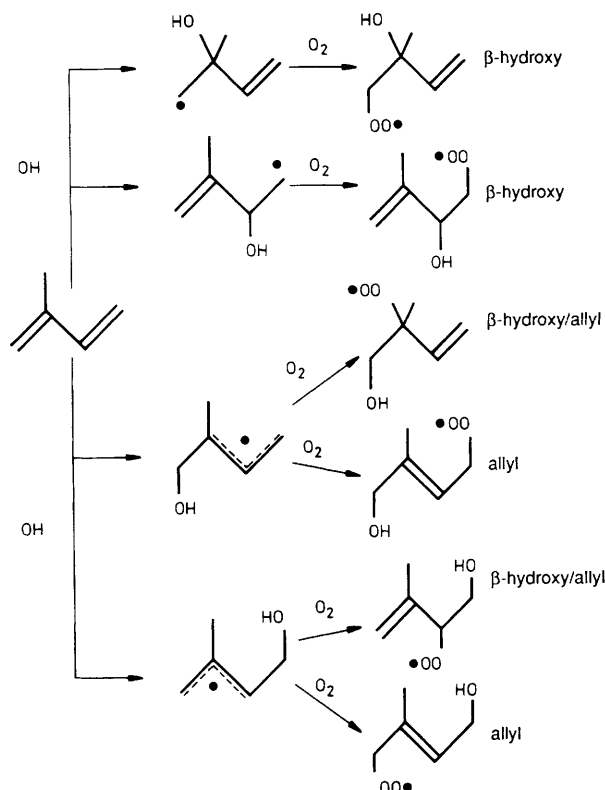


Fig. 1 Organic peroxy radicals formed from the OH-initiated oxidation of isoprene

six possible classes of peroxy radical, as shown in Fig. 1. These radicals contain either the ' $\beta$ -hydroxy' functionality, the 'allyl' functionality, or both. Clearly, it is important to be able to assess the influence of these functional groups on the kinetics and mechanisms of the possible competing reactions (1)–(4). Recent studies from this laboratory<sup>11,12</sup> of the  $\beta$ -hydroxy peroxy radical  $HOCH_2CH_2O_2$  have shown that reactions (2) and (3) have rate coefficients of  $1.2 \times 10^{-11}$  and  $2.2 \times 10^{-12} \text{ cm}^3 \text{ molecule}^{-1} \text{ s}^{-1}$ , respectively. These are greater by factors of *ca.* 2 and 30 than the coefficients for the corresponding reactions of  $C_2H_5O_2$ .<sup>3</sup> In contrast, reaction (1) occurs at approximately the same rate for both  $C_2H_5O_2$  and  $HOCH_2CH_2O_2$ .

There are currently no published investigations of any of reactions (1)–(4) for peroxy radicals containing the allyl functionality. In this paper, we present the results of laser flash photolysis experiments to obtain UV spectral and self-reaction kinetic data for the allyl peroxy radical,  $CH_2=CHCH_2O_2$ . As part of this work the UV spectrum and recombination kinetics of the allyl radical were also quantitatively investigated. For simplicity, the allyl radical is written as  $CH_2=CHCH_2$  throughout this paper. It should be noted, however, that the unpaired electron is delocalised over the carbon chain (as demonstrated for the allyl-type radicals in Fig. 1). The long pathlength FTIR spectroscopy technique was employed to identify and quantify the products of the self-reaction of  $CH_2=CHCH_2O_2$ , allowing the reaction channels and branching ratios to be defined. The kinetic and mechanistic data obtained for  $CH_2=CHCH_2O_2$  along with those measured previously for  $HOCH_2CH_2O_2$ <sup>11,12</sup> are used to infer average rate coefficients for the  $RO_2$  radicals produced in the OH radical-initiated oxidation of isoprene. A simple box model of the planetary boundary layer is used to demonstrate the potential impact of elevated concentrations of isoprene [3 ppbv] on ambient levels of OH,  $HO_2$ ,  $RO_2$ ,  $O_3$  and the  $NO_x$  species.

## Experimental

The laser flash photolysis–UV absorption apparatus employed in the present work was used in two experimental configurations. In each configuration, radicals are produced inside a cylindrical silica reaction vessel by irradiating an appropriate precursor gas mixture flowing slowly through the vessel with 193 or 248 nm radiation from an excimer laser. The radicals produced by the laser pulse were detected by time-resolved UV absorption spectroscopy using broad-band emission from a high brightness deuterium lamp as the monitoring beam.

In the first configuration, which has been described in detail previously,<sup>12</sup> the laser beam was expanded so that it uniformly irradiated the gas mixture through the side wall of a reaction vessel 30 cm in length and 3 cm in diameter. The monitoring beam made four traversals of the vessel length using internally mounted White optics. The effective pathlength illuminated by the laser radiation was found to be  $85 \pm 5 \text{ cm}$ .<sup>12</sup>

In the second configuration, shown schematically in Fig. 2, the laser beam is passed along the axis of a longer reaction vessel (1 m in length, 25 mm i.d.) counter-propagating the monitoring beam which makes only one pass along the vessel axis. This arrangement was set up primarily to allow the reaction vessel to be cooled by surrounding it with an outer cooling jacket or to be heated by installing it in a furnace. The rectangular profile of the laser beam was slightly expanded and re-collimated by means of cylindrical lenses to produce a square profile slightly larger than the cross-section of the vessel. This ensured that the inner volume of the vessel was irradiated homogeneously. The fluence of the laser beam entering the vessel in this configuration was typically  $15 \text{ mJ cm}^{-2}$  compared with *ca.*  $2 \text{ mJ cm}^{-2}$  with the first configuration. The laser and monitoring beams enter and exit the vessel through two removable end-window pieces with O-ring seals. Each piece consisted of an evacuated silica tube (20 cm in length, 23 mm o.d.), sealed with 1 mm thick UV-grade silica flats fused to the tube at Brewster angle to the vessel axis. When mounted to the vessel, the inner windows of each end-piece were thus situated inside the vessel, *ca.* 10 cm from the end, defining an optical pathlength for the reaction volume of 81 cm. Although not relevant to this investigation, the end-pieces were designed primarily to ensure that the reaction volume was at uniform temperature for high- and low-temperature kinetic studies.

With the reaction vessel mounted with its axis orthogonal to the laser axis, the spatially overlapping laser and monitoring beams, respectively, entering and exiting the vessel could be separated by means of suprasil flats with wavelength discriminating reflection coatings. For 193 nm photolysis a coating was used which reflected >99% of the laser beam into the vessel, but transmitted >90% of the monitoring beam exiting the vessel in the spectral region at  $\lambda \geq 215 \text{ nm}$  (193 nm high-reflector). Complete separation of the 248 nm radiation from the monitoring beam could not be achieved because the laser wavelength fell within the monitoring spectral range of interest. Therefore, for these experiments a partial reflector was used, which reflected 50% of the laser beam into the vessel (the transmitted component being terminated) and transmitted 30–55% of the monitoring beam at  $\lambda = 300\text{--}210 \text{ nm}$  exiting the vessel for collection.

The transmitted monitoring beams were focused onto the 1.25 mm entrance slit of a monochromator and detected by a photomultiplier. The spectral resolution in all experiments was *ca.* 2 nm. Signals from the photomultiplier were captured on a digital storage oscilloscope, processed, accumulated and stored on a microcomputer for analysis as described pre-

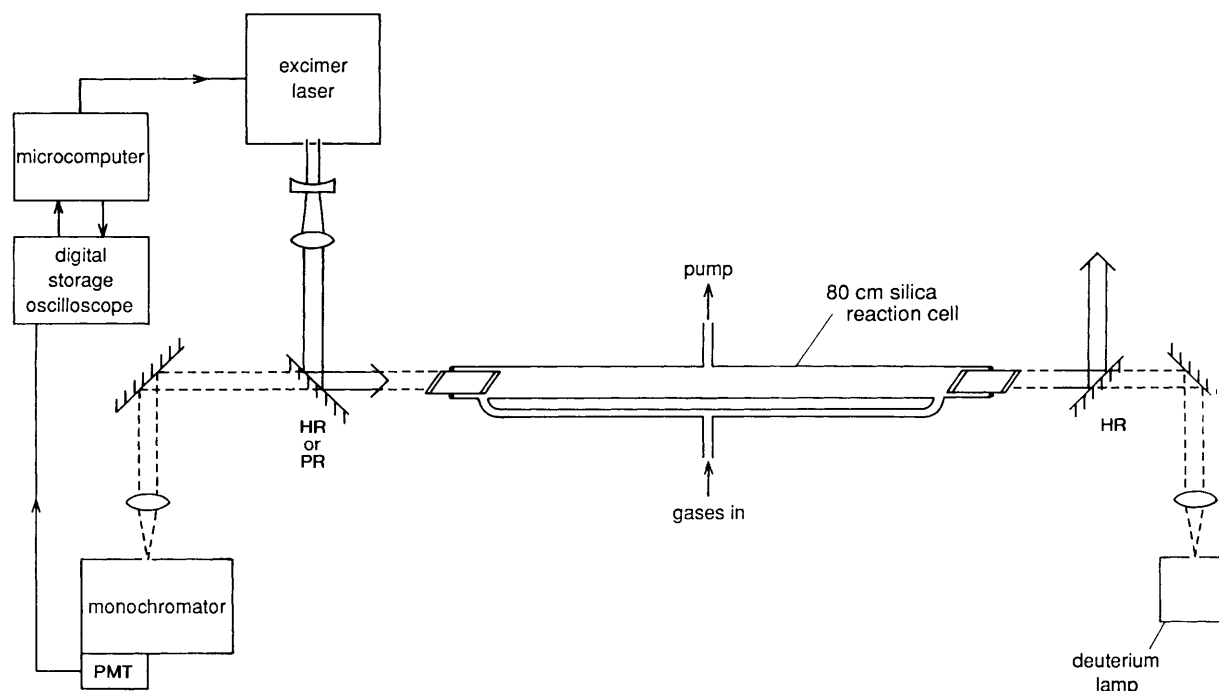


Fig. 2 Schematic diagram of laser flash photolysis-UV absorption apparatus; HR = 193 nm high reflector and PR = 248 nm 50% reflector

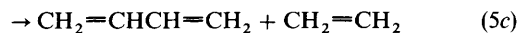
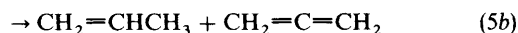
viously.<sup>12</sup> Signal *vs.* time profiles for 20–400 laser shots fired at a repetition rate of one pulse every 5 s were accumulated to provide averaged absorption *vs.* time profiles. With a gas residence time of *ca.* 7 s in the vessel this ensured that for the majority of the time a fresh sample of gas was photolysed by each laser shot.

For the 193 nm photolysis experiments it was necessary to minimise the length of the path in which the laser and monitoring beams overlap outside the vessel in order to minimise the contribution to the absorption profile by the small amount of ozone formed in the path of the laser beam by photolysis of the atmospheric oxygen. This was accomplished by placing a second 193 nm reflector at the end of the vessel where the laser beam exits and by mounting both 193 nm reflectors as close as possible to the outer window of the evacuated end-pieces. The maximum absorbance due to O<sub>3</sub> formation by the laser pulse was <0.2% and was subtracted from the stored absorption–time profiles.

In all experiments using the second configuration it was necessary to ensure that the absorbance at the laser wavelength due to the radical precursor was sufficiently low so as to avoid significant complications to the kinetics of the radical as a result of radical concentration gradients along the length of the vessel due to attenuation of the laser intensity. Calculations showed that the observed decay of the transient absorbance signal due to a radical reacting with second-order kinetics would not deviate from second-order behaviour if the absorbance at the laser wavelength due to its precursor was ≤0.5. Furthermore, the rate coefficient derived from second-order analysis of the observed absorption *vs.* time profile would be the same as the true rate coefficient for the reaction.

The long pathlength FTIR apparatus comprises a cylindrical silica reaction vessel (volume = 10 dm<sup>3</sup>, i.d. = 10 cm), equipped with internal White optics. Most experiments were performed with 16 traversals of the IR monitoring beam over the 80 cm base path. Measurements were made in the range 400–4000 cm<sup>-1</sup> with a resolution of 1 cm<sup>-1</sup>, using a Mattson Instruments FTIR spectrometer (4020 Galaxy Series).

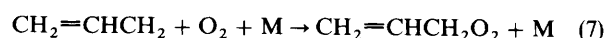
Two sources of CH<sub>2</sub>=CHCH<sub>2</sub> were used in the present study. For the laser flash photolysis experiments, the 193 nm photolysis of hexa-1,5-diene provides a convenient source, which has been well characterised by Van den Bergh and Callear<sup>13</sup> and by Pilling and co-workers.<sup>14,15</sup>



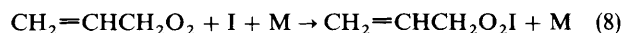
The end product analysis of Tulloch *et al.*<sup>14</sup> allowed the relative importance of the photolysis channels to be established as 68 : 27 : 2.5 : 2.5 at 193 nm. Thus CH<sub>2</sub>=CHCH<sub>2</sub> represents 68% of the total products, and 96% of the radical products. The photolysis of allyl iodide (CH<sub>2</sub>=CHCH<sub>2</sub>I) was used as a source of CH<sub>2</sub>=CHCH<sub>2</sub> in both laser experiments (248 nm photolysis), and in FTIR product experiments, where the photolysis was achieved using three low-pressure mercury tubes (Philips TUV 40W) emitting mainly at 253.7 nm:



Addition of O<sub>2</sub> to the reaction mixtures allowed formation of CH<sub>2</sub>=CHCH<sub>2</sub>O<sub>2</sub>:



For the kinetics studies, the 193 nm photolysis of hex-1,5-diene was used exclusively as the source of CH<sub>2</sub>=CHCH<sub>2</sub>O<sub>2</sub>. Possible kinetic and spectroscopic complications using the allyl iodide system arise from the production of CH<sub>2</sub>=CHCH<sub>2</sub>O<sub>2</sub>I from the addition reaction of the peroxy radical with I atoms, as observed previously for CH<sub>3</sub>O<sub>2</sub> and HOCH<sub>2</sub>CH<sub>2</sub>O<sub>2</sub>.<sup>11</sup>



However, on the basis of the previous work,<sup>11</sup> the influence of this reaction on the distribution of oxidation products in a steady-state photolysis system is believed to be minor owing to the continuous presence of a significant concentration of I atoms allowing regeneration of the peroxy radical:



Thus, the peroxy radical catalyses the recombination of I atoms, but is not itself removed by the interaction. Consequently the photolysis of allyl iodide in the presence of O<sub>2</sub> provides a suitable source of CH<sub>2</sub>=CHCH<sub>2</sub>O<sub>2</sub> for FTIR end-product investigation.

Kinetics measurements were made using flowing gas mixtures. The product measurements were made in stopped flow mode. The constituent gases (N<sub>2</sub> and O<sub>2</sub>) were either regulated using mass flow controllers (MKS, Type 261) or were monitored using mass flow meters (Tylan, 280 series) or calibrated rotameters. In each experiment, either hexa-1,5-diene or allyl iodide was admitted to the vessel by diverting a proportion of the gas flow through a bubbler containing the appropriate liquid. The total pressures in the reaction vessels were measured using capacitance manometers (MKS Baratron Type 222BA). Experiments were performed at, or slightly in excess of, atmospheric pressure (740–800 Torr†), and at room temperature ( $T = 296 \pm 2$  K).

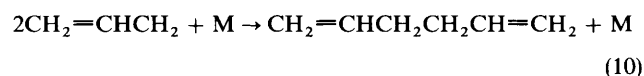
The materials used in the present study were obtained from the following sources: N<sub>2</sub> (Air Products, high purity), O<sub>2</sub> (BOC breathing grade), hexa-1,5-diene (Aldrich, 98%), allyl iodide (Aldrich, 98%), allyl alcohol (Aldrich, 99+%), acrolein (Aldrich, 97%), CH<sub>3</sub>I (BDH, 99%). In flowing gas mixtures the materials were used as received. However, samples of allyl iodide and CH<sub>3</sub>I were further purified by trap-to-trap distillation for the purpose of measuring their UV absorption spectra.

## Results

### UV Absorption Spectrum and Self-reaction Kinetics of CH<sub>2</sub>=CHCH<sub>2</sub>

#### 193 nm Laser Flash Photolysis of Hexa-1,5-diene-N<sub>2</sub>

Absorption-time traces obtained from the 193 nm flash photolysis of flowing hexa-1,5-diene-N<sub>2</sub> mixtures were recorded at 2.5 nm intervals over the wavelength range 210–232.5 nm using both experimental configurations. Examples of traces are displayed in Fig. 3. No difference was observed between the results obtained in the two configurations. The variation of maximum absorbance with wavelength provided a relative spectrum in good agreement with the results of Van den Bergh and Callear,<sup>13</sup> which is attributed to the allyl radical (CH<sub>2</sub>=CHCH<sub>2</sub>) produced by reaction (5a). Following the initial rise time, which results from scattered light after the laser flash, CH<sub>2</sub>=CHCH<sub>2</sub> displayed second-order kinetic behaviour, as demonstrated by the linearity of the (absorbance)<sup>-1</sup> vs. time plot shown in Fig. 3B. This indicates removal by a rapid self-reaction, which is dominated by the recombination channel (10):<sup>14</sup>



The decay traces were analysed by a non-linear least-squares fitting procedure to allow determination of  $k_{10}/\sigma$  at each monitoring wavelength. The results provided a value of  $k_{10}/\sigma$  (220 nm) of  $(5.1 \pm 0.4) \times 10^5 \text{ cm s}^{-1}$  near the absorption maximum.

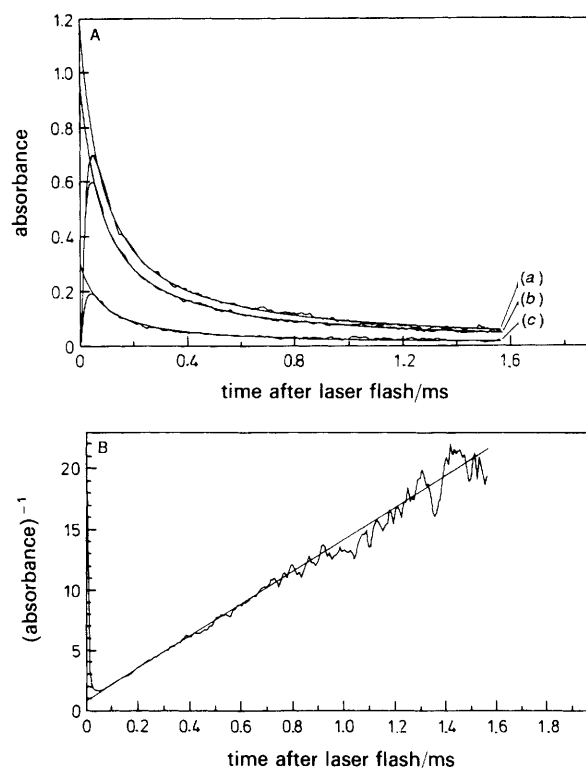


Fig. 3 Decay traces measured for the allyl radical (CH<sub>2</sub>=CHCH<sub>2</sub>) formed from the 193 nm photolysis of hexa-1,5-diene-N<sub>2</sub> mixtures. A, absorbance-time traces at (a) 220, (b) 225 and (c) 230 nm. B, (absorbance)<sup>-1</sup>-time trace at 225 nm

An attempt was made to calibrate the relative spectrum by adding I<sub>2</sub> to the reaction mixture to scavenge CH<sub>2</sub>=CHCH<sub>2</sub>, so that the product, allyl iodide (CH<sub>2</sub>=CHCH<sub>2</sub>I), could be used as an actinometer:



Unfortunately, the concentration of I<sub>2</sub> required for reaction (11) to dominate over the rapid recombination reaction (10) (*ca.*  $1 \times 10^{16} \text{ molecule cm}^{-3}$ ) resulted in severe attenuation of the laser photolysis radiation at 193 nm, which inhibited the initial formation of CH<sub>2</sub>=CHCH<sub>2</sub>. Consequently, almost no signal due to the formation of the product allyl iodide could be observed.

#### 248 nm Laser Flash Photolysis of Allyl Iodide-N<sub>2</sub>

Preliminary experiments were performed to measure the UV absorption spectrum of allyl iodide. The sample received was found to contain a minor volatile impurity, which was identified as acrolein by FTIR measurement (see below). After purification by trap-to-trap distillation, accurately measured pressures of allyl iodide of up to *ca.* 5 Torr were admitted into a 5 cm pathlength cell. Diode array spectral measurements were made by the method described in detail previously,<sup>16</sup> and the resultant spectrum of allyl iodide is shown in Fig. 4 with the cross-sections given in Table 1. Associated measurements of the spectrum of CH<sub>3</sub>I obtained by the same methodology are displayed for comparison.

Absorption-time traces were measured at various wavelengths in the range 210–230 nm following the 248 nm flash photolysis of flowing allyl iodide-N<sub>2</sub> mixtures. Examples are shown in Fig. 5. The variation of the signal with wavelength did not follow the relative spectrum of CH<sub>2</sub>=CHCH<sub>2</sub> measured in the hexa-1,5-diene experiments, owing to a significant negative contribution made over the complete

† 1 Torr = (101 325/760) Pa.

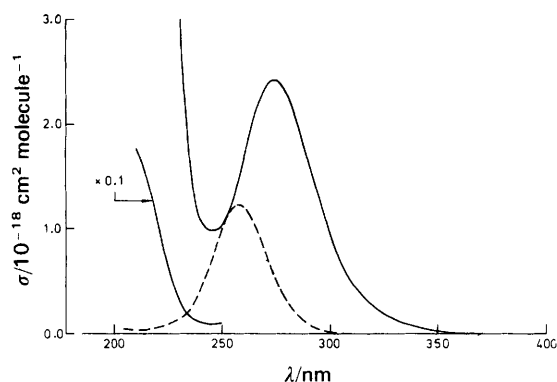


**Fig. 4** UV absorption spectra of (broken line)  $\text{CH}_3\text{I}$  ( $\sigma = 1.22 \times 10^{-18} \text{ cm}^2 \text{ molecule}^{-1}$  at  $\lambda_{\text{max}} = 257.9 \text{ nm}$ ) and (solid line)  $\text{CH}_2=\text{CHCH}_2\text{I}$  ( $\sigma = 2.42 \times 10^{-18} \text{ cm}^2 \text{ molecule}^{-1}$  at  $\lambda_{\text{max}} = 269.1 \text{ nm}$ )

wavelength range by the removal of allyl iodide resulting from the laser photolysis. At wavelengths below 215 nm, the negative signal due to removal of allyl iodide was comparable to, or exceeded that due to the production of  $\text{CH}_2=\text{CHCH}_2$ . However, inspection of the decay traces at longer times revealed almost no negative offset at any wavelength (see Fig. 5) suggesting that the allyl iodide was almost totally regenerated. This was confirmed by measurements made at the peak of the allyl iodide spectrum (269 nm), where  $\text{CH}_2=\text{CHCH}_2$  radicals do not contribute to the absorption. It was also clear that  $\text{CH}_2=\text{CHCH}_2$  was being removed significantly more

**Table 1** UV absorption cross-sections measured for  $\text{CH}_2=\text{CHCH}_2\text{I}$  and  $\text{CH}_3\text{I}$

$\lambda/\text{nm}$	$\sigma/10^{-20} \text{ cm}^2 \text{ molecule}^{-1}$	
	$\text{CH}_2=\text{CHCH}_2\text{I}$	$\text{CH}_3\text{I}$
205	—	4.9
210	1767	3.4
215	1477	4.9
220	1072	6.9
225	649.0	9.2
230	340.2	12.8
235	173.9	21.8
240	107.6	40.3
245	100.8	68.1
250	126.6	98.0
255	166.9	118.3
257.9	—	121.8
260	206.8	119.9
265	234.4	103.3
269.1	242.3	—
270	241.3	77.4
275	228.8	51.5
280	201.5	31.0
285	164.8	16.8
290	128.8	8.54
295	96.7	4.31
300	70.4	2.22
305	50.8	1.19
310	36.9	0.68
315	26.4	0.38
320	18.9	0.24
325	13.6	0.14
330	9.8	0.07
335	6.7	0.02
340	4.5	—
345	2.9	—
350	1.9	—
355	1.2	—
360	0.6	—
365	0.2	—

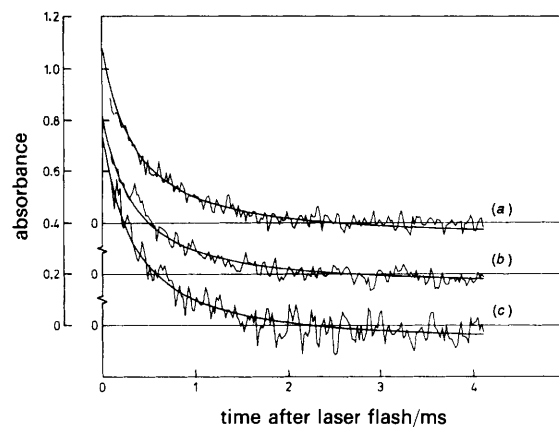
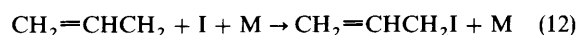


**Fig. 5** Decay traces measured at (a) 222.5, (b) 225.0 and (c) 220.0 nm following the 248 nm photolysis of allyl iodide- $\text{N}_2$  mixtures

rapidly than could be accounted for by the recombination reaction (10). The most probable explanation for these observations is the existence of a rapid recombination reaction of  $\text{CH}_2=\text{CHCH}_2$  and I atoms competing with reaction (10):



In principle, it should be possible to determine the absolute cross-sections for  $\text{CH}_2=\text{CHCH}_2$  from the extent to which the removal of allyl iodide distorts the observed variation of initial signal with wavelength away from the  $\text{CH}_2=\text{CHCH}_2$  spectral shape. However, the magnitude of the optical absorbances immediately after the flash could not be measured, because scattered laser light and emissions from the vessel walls and windows induced by the laser, interfered with the absorption measurements for the first 0.1 ms after the flash. During this time  $\text{CH}_2=\text{CHCH}_2$  had decayed significantly from its initial concentration, owing to the rapid reaction (12), so this simple analysis was precluded. Instead, the decay traces were analysed using the numerical integration program FACSIMILE.<sup>17</sup> Sets of data measured at three wavelengths in the range 217.5–230 nm, under identical experimental conditions, were simulated using the chemical mechanism shown in Table 2, incorporating the relative  $\text{CH}_2=\text{CHCH}_2$  spectrum measured in the hexa-1,5-diene experiments, and the absolute allyl iodide spectrum. The combined data in each set contained sufficient information to allow optimisation of three parameters, by simultaneous fitting of the three decay traces. These parameters were  $\sigma(220 \text{ nm})$  for  $\text{CH}_2=\text{CHCH}_2$ ,  $k_{12}$  and the initial radical concentration. Examples of fits to the data are shown in Fig. 5. The

**Table 2** Reactions and rate coefficients used to simulate absorption-time traces measured during the flash photolysis of allyl iodide- $\text{N}_2$  mixtures

reaction	rate coefficient
$\text{CH}_2=\text{CHCH}_2\text{I} + h\nu \rightarrow \text{CH}_2=\text{CHCH}_2 + \text{I}$	instantaneous <sup>a</sup>
$2\text{CH}_2=\text{CHCH}_2 (+\text{M}) \rightarrow$	
$\text{CH}_2=\text{CHCH}_2\text{CH}_2\text{CH}=\text{CH}_2 (+\text{M})$	$5.1 \times 10^5 \sigma(220 \text{ nm})^b$
$\text{CH}_2=\text{CHCH}_2 + \text{I} (+\text{M}) \rightarrow$	
$\text{CH}_2=\text{CHCH}_2\text{I} (+\text{M})$	varied (see text)
$\text{I} + \text{I} (+\text{M}) \rightarrow \text{I}_2 (+\text{M})$	$2.5 \times 10^{-13} \text{ cm}^3 \text{ molecule}^{-1} \text{ s}^{-1} \text{ c}$

<sup>a</sup> The initial loss of allyl iodide,  $\Delta[\text{CH}_2=\text{CHCH}_2\text{I}]$ , was assumed equivalent to the initial concentrations  $[\text{CH}_2=\text{CHCH}_2]_i$  and  $[\text{I}]_i$ . This initial concentration was a fitted parameter. <sup>b</sup> The value of  $\sigma(220 \text{ nm})$  was a fitted parameter. Units of rate coefficient  $\text{cm}^3 \text{ molecule}^{-1} \text{ s}^{-1}$ . <sup>c</sup> Units,  $\text{cm}^3 \text{ molecule}^{-1} \text{ s}^{-1}$ . Value taken from ref. 18.

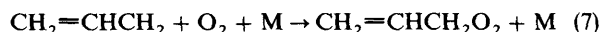
**Table 3** Absolute absorption cross-sections determined for  $\text{CH}_2=\text{CHCH}_2$ 

$\lambda/\text{nm}$	$\sigma/10^{-17} \text{ cm}^2 \text{ molecule}^{-1}$
210	0.61
212.5	1.57
215	2.73
217.5	4.08
220	5.80
222.5	6.14
225	5.09
227.5	2.58
230	1.71
232.5	0.59

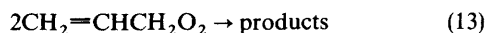
following mean values were obtained from two sets of three decay traces, the quoted error limits being the statistical errors in the fits ( $1\sigma$ ):  $\sigma(220 \text{ nm}) = (5.8 \pm 0.8) \times 10^{-17} \text{ cm}^2 \text{ molecule}^{-1}$ ; and  $k_{12} = (1.6 \pm 0.6) \times 10^{-10} \text{ cm}^3 \text{ molecule}^{-1} \text{ s}^{-1}$ . Corresponding cross-sections for  $\text{CH}_2=\text{CHCH}_2$  over the range 210–232.5 nm are displayed in Table 3 and Fig. 6. Using the value of  $k_{10}/\sigma(220 \text{ nm})$  measured in the hexa-1,5-diene experiments gives the value of  $k_{10} = (3.0 \pm 0.5) \times 10^{-11} \text{ cm}^3 \text{ molecule}^{-1} \text{ s}^{-1}$ .

#### UV Absorption Spectrum and Self-reaction Kinetics of $\text{CH}_2=\text{CHCH}_2\text{O}_2$

The addition of  $10^{18} \text{ molecule cm}^{-3} \text{ O}_2$  to the hexa-1,5-diene system allowed rapid conversion of  $\text{CH}_2=\text{CHCH}_2$  into  $\text{CH}_2=\text{CHCH}_2\text{O}_2$ :



Absorption-time traces were recorded in the wavelength range 210–300 nm (examples are shown in Fig. 7), the observed variation of the initial absorbance with wavelength being typical of an organic peroxy radical (*i.e.* due to  $\text{CH}_2=\text{CHCH}_2\text{O}_2$ ), with a maximum at 235 nm (see Table 4). A plot of  $(\text{absorbance})^{-1}$  vs. time for a dataset recorded at 235 nm (Fig. 7B) is linear, indicating that  $\text{CH}_2=\text{CHCH}_2\text{O}_2$  was displaying second-order kinetic behaviour. This suggests that the peroxy radical was removed primarily by its self-reaction:



Second-order kinetics were observed at all wavelengths investigated. Non-linear least-squares analysis of the decay traces in the range 220–270 nm provided values of the ratio  $k_{13\text{obs}}/\sigma_\lambda$  (where  $k_{13\text{obs}}$  is the observed second-order rate coefficient) at the monitoring wavelength which varied

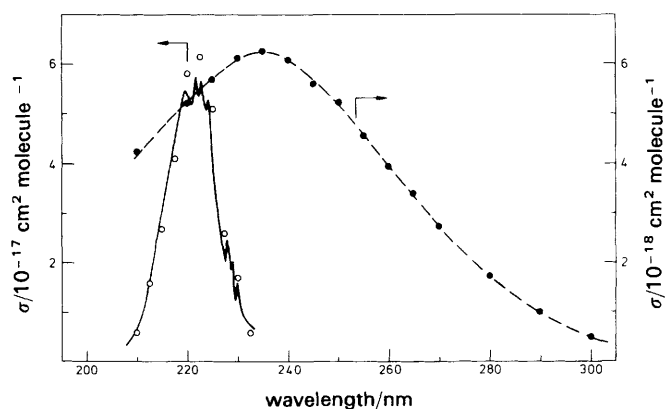


**Fig. 6** UV absorption spectra measured for  $\text{CH}_2=\text{CHCH}_2$  (○) and  $\text{CH}_2=\text{CHCH}_2\text{O}_2$  (●). The  $\text{CH}_2=\text{CHCH}_2$  spectrum reported by Van den Bergh and Callear<sup>13</sup> (solid line) is also shown

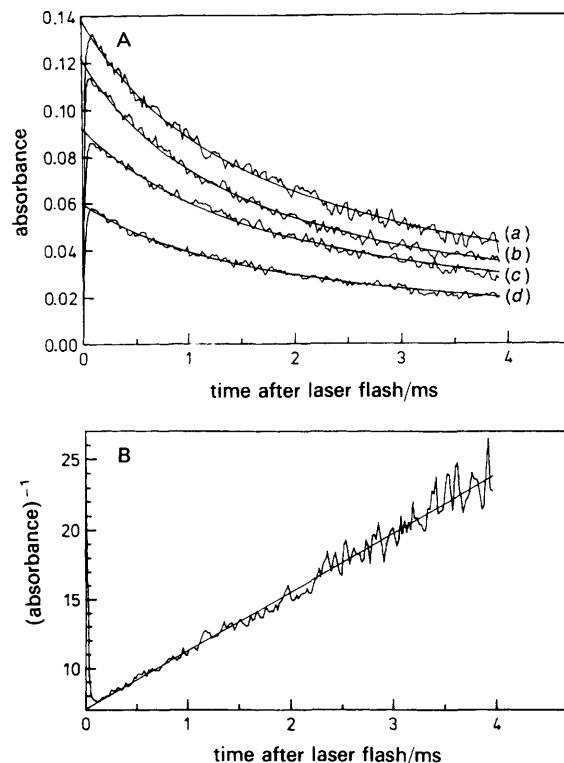


**Fig. 7** Decay traces measured for the allyl peroxy radical ( $\text{CH}_2=\text{CHCH}_2\text{O}_2$ ) formed from the 193 nm photolysis of hexa-1,5-diene- $\text{O}_2$  mixtures. A, absorbance-time traces at (a) 235, (b) 250, (c) 260 and (d) 270 nm. B,  $(\text{absorbance})^{-1}$ -time trace at 235 nm

inversely with the initial absorbance (see Table 4), confirming that only one species was absorbing significantly at these wavelengths. The absorption spectrum of  $\text{CH}_2=\text{CHCH}_2\text{O}_2$  was calibrated relative to that measured for  $\text{CH}_2=\text{CHCH}_2$  by performing three pairs of experiments in the presence and absence of  $\text{O}_2$  whilst monitoring at 220 nm. The resultant relative cross-section at 220 nm,  $\sigma(\text{CH}_2=\text{CHCH}_2\text{O}_2)/\sigma(\text{CH}_2=\text{CHCH}_2)$ , was  $(8.9 \pm 0.6) \times 10^{-2}$ , leading to the absolute cross-section for  $\text{CH}_2=\text{CHCH}_2\text{O}_2$  at 220 nm of  $\sigma(220 \text{ nm}) = (5.2 \pm 0.8) \times 10^{-18} \text{ cm}^2 \text{ molecule}^{-1}$ . Corresponding cross-sections for the complete wavelength range are given in Table 4, together with values of  $k_{13\text{obs}}$  determined from the measured values of  $k_{13\text{obs}}/\sigma_\lambda$ . The resultant mean value is  $k_{13\text{obs}} = (1.1 \pm 0.2) \times 10^{-12} \text{ cm}^3 \text{ molecule}^{-1} \text{ s}^{-1}$

**Table 4** Values of  $\sigma$ ,  $k_{13\text{obs}}/\sigma$  and  $k_{13\text{obs}}$  determined for  $\text{CH}_2=\text{CHCH}_2\text{O}_2$

$\lambda/\text{nm}$	$\sigma/10^{-18} \text{ cm}^2 \text{ molecule}^{-1}$	$(k_{13\text{obs}}/\sigma)/10^5 \text{ cm}^3 \text{ s}^{-1}$	$k_{13\text{obs}}/10^{-13} \text{ cm}^3 \text{ molecule}^{-1} \text{ s}^{-1}$
210	4.28	—	—
220	5.20	2.11	11.0
225	5.80	1.89	11.0
		2.09	12.1
230	6.09	1.80	11.0
		1.78	10.8
235	6.17	1.72	10.6
240	6.09	1.94	11.8
245	5.60	1.77	9.9
250	5.26	2.15	11.3
255	4.56	2.38	10.9
260	3.96	2.54	10.1
265	3.42	3.38	11.6
270	2.75	3.66	10.1
280	1.73	—	—
290	0.90	—	—
300	0.43	—	—

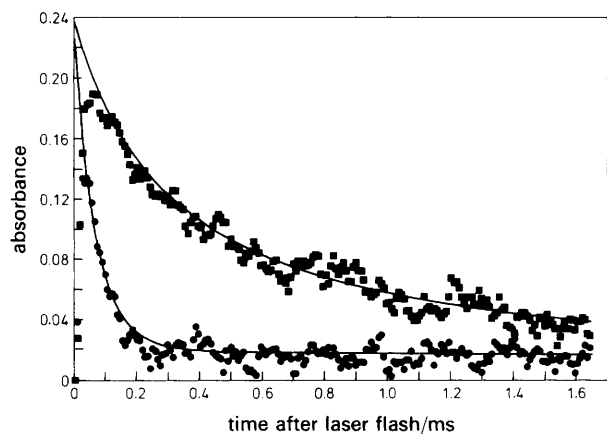


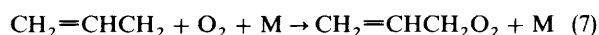
**Fig. 8** Decay traces measured at 220 nm following the 193 nm photolysis of hexa-1,5-diene in the absence of  $O_2$  (■) and in the presence of  $2.1 \times 10^{16}$  molecule  $cm^{-3}$   $O_2$  (●). The conversion of  $CH_2=CHCH_2$  into  $CH_2=CHCH_2O_2$  is apparent

$s^{-1}$ . The UV absorption spectrum of  $CH_2=CHCH_2O_2$  is also displayed in Fig. 6 along with the  $CH_2=CHCH_2$  spectrum.

Several experiments were performed with much lower  $O_2$  concentrations (*ca.*  $10^{16}$  molecule  $cm^{-3}$ ), allowing the conversion of the more strongly absorbing  $CH_2=CHCH_2$  into  $CH_2=CHCH_2O_2$  to be observed (see Fig. 8). Non-linear least-squares fitting of these data using the cross-sections for the two radicals and the values of  $k_{10}$  and  $k_{13obs}$  determined above, indicated that  $k_7$  lies in the range  $(6 \pm 2) \times 10^{-13}$   $cm^3$  molecule $^{-1}$   $s^{-1}$ .

### Products of the Oxidation of $CH_2=CHCH_2$

To assist in the elucidation of the oxidation mechanism for  $CH_2=CHCH_2$ , the 253.7 nm photolysis of allyl iodide in the presence of various concentrations of  $O_2$  was investigated by long pathlength FTIR spectroscopy. Initially, the disappearance rate of allyl iodide during photolysis was analysed as a function of  $[O_2]$ , using the IR band at  $670$   $cm^{-1}$ . log-linear plots of the observed decay (Fig. 9) indicate that removal was first order at high  $[O_2]$  ( $2.4 \times 10^{19}$  molecule  $cm^{-3}$ ), and the observed disappearance is attributed to the photolysis reaction (with  $k_6 = 6.3 \times 10^{-3}$   $s^{-1}$ ) followed by scavenging of  $CH_2=CHCH_2$  by reaction with  $O_2$ :



At lower  $[O_2]$ , first-order decay was no longer observed, with the measured decay rate reduced at longer photolysis times. This is explained by the accumulation of  $I_2$  in the system from the recombination of  $I$  atoms, which provides a competing reaction for  $CH_2=CHCH_2$  at lower  $[O_2]$ , leading to the regeneration of allyl iodide:



The data obtained at  $[O_2] = 4.5 \times 10^{17}$  and  $1.3 \times 10^{17}$  molecule  $cm^{-3}$  were simulated using this simple mechanism to obtain an optimised value of  $k_{11}/k_7 = (20 \pm 7)$  (see Fig. 9). Using the value of  $k_7 = (6 \pm 2) \times 10^{-13}$   $cm^3$  molecule $^{-1}$   $s^{-1}$ , presented above, leads to  $k_{11} = (1.2 \pm 0.6) \times 10^{-11}$   $cm^3$  molecule $^{-1}$   $s^{-1}$ . It should be noted that, even at the lowest concentration of  $O_2$ , the reactions of  $CH_2=CHCH_2$  with itself and  $I$  atoms, which were important in the laser flash photolysis experiments, are unable to compete with reactions

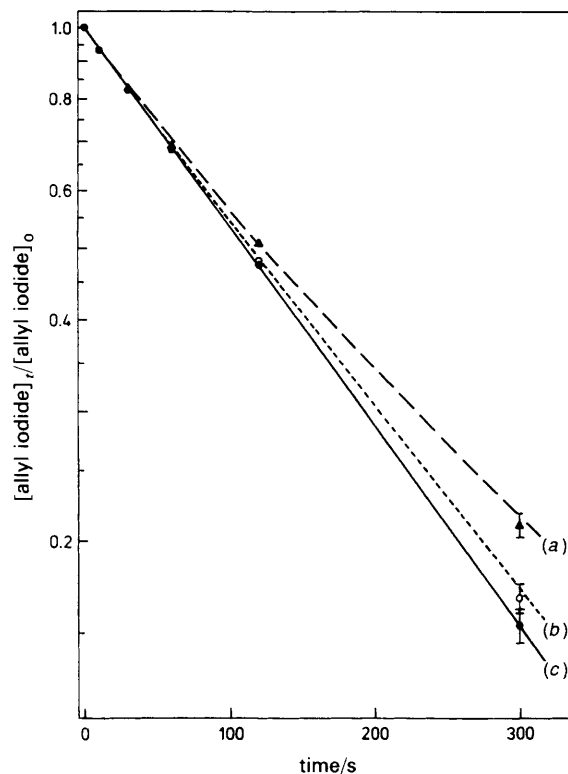
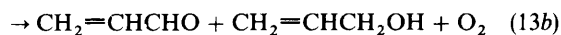
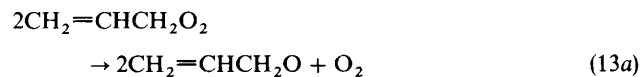


**Fig. 9** log-linear plots of the decay of allyl iodide during photolysis at 253.7 nm. (a)  $[O_2] = 1.3 \times 10^{17}$ ; (b)  $[O_2] = 4.5 \times 10^{17}$ ; and (c)  $[O_2] = 2.4 \times 10^{19}$  molecule  $cm^{-3}$ . Lines are results of simulations (see text)

(7) and (11) under the low intensity photolysis conditions of this product study.

The products of the photolysis of allyl iodide in the presence of  $2.4 \times 10^{19}$  molecule  $cm^{-3}$   $O_2$  were first considered. In all experiments, low concentrations of acrolein,  $CH_2=CHCHO$ , were present initially as an impurity (*ca.* 2–5% of the allyl iodide concentration). This has a negligible effect on the system, since  $CH_2=CHCHO$  is not photolysed significantly by 253.7 nm radiation.<sup>19</sup> The major photolysis products identified were  $CH_2=CHCHO$  itself, and allyl alcohol,  $CH_2=CHCH_2OH$  (see Fig. 10), which may both be formed from the terminating channel (13b) of the self-reaction of  $CH_2=CHCH_2O_2$ :



$CH_2=CHCHO$  may also be formed by subsequent reaction of the alkoxy radical,  $CH_2=CHCH_2O$ , formed in the propagating channel (13a):



The observed yields of  $CH_2=CHCHO$  were always much greater than those of  $CH_2=CHCH_2OH$ , indicating a significant contribution of channel (13a) to the self-reaction. As shown in Fig. 10, the product sample spectrum was dominated by features due to  $CH_2=CHCHO$ , although  $CH_2=CHCH_2OH$  bands are also clearly discernible. After subtraction of  $CH_2=CHCHO$  and  $CH_2=CHCH_2OH$  reference spectra from the product spectrum, the residual spectrum contained characteristic 'allyl' bands and additional features at *ca.* 840 and 3590  $cm^{-1}$ . These are attributed to the hydroperoxide species  $CH_2=CHCH_2O_2H$  formed from the

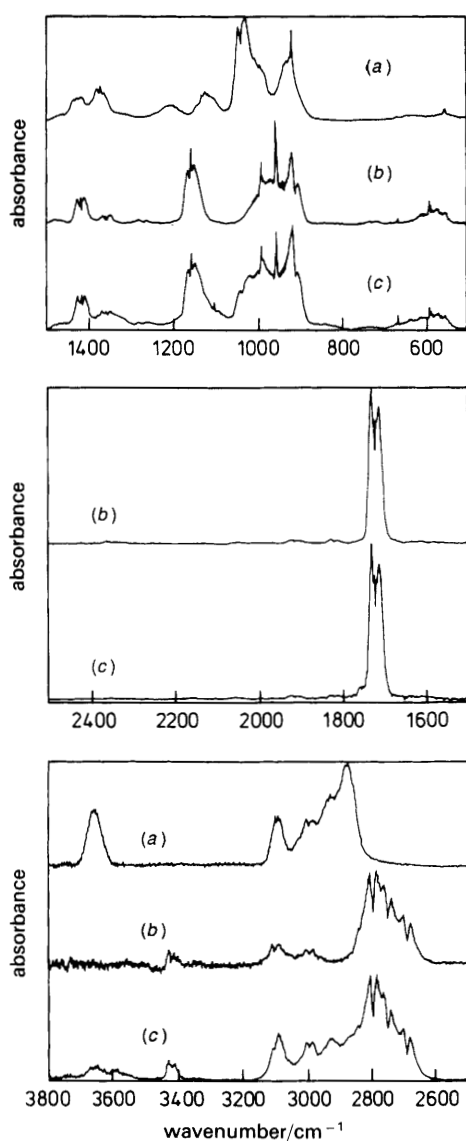
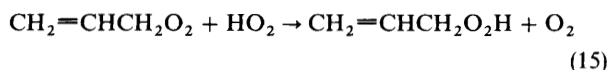


**Fig. 10** FTIR spectrum of products of 253.7 nm photolysis of (c) allyl iodide- $O_2$  mixture compared with reference spectra of (a) allyl alcohol ( $CH_2=CHCH_2OH$ ) and (b) acrolein ( $CH_2=CHCHO$ ). Features due to residual allyl iodide have been subtracted

reaction of  $HO_2$  produced in reaction (14) with  $CH_2=CHCH_2O_2$ :



There were no features to suggest the existence of alternative reactions for  $CH_2=CHCH_2O$  competing with reaction (14) at this  $O_2$  concentration, such as thermal decomposition, which would yield HCHO both directly and through subsequent reactions of the vinyl radical,  $CH_2=CH$ .<sup>19,20</sup>



With the assumption that there are no other sources of  $CH_2=CHCHO$  and  $CH_2=CHCH_2OH$  in this system, the relative yield  $[CH_2=CHCH_2OH]/[CH_2=CHCHO]$  ( $=x$ ), may therefore be used to calculate the branching ratio for reaction (13),  $\alpha_{13} = k_{13a}/(k_{13a} + k_{13b}) = (1-x)/(1+x)$ . The results of three experiments performed with high  $[O_2]$  ( $2.4 \times 10^{19}$  molecule  $cm^{-3}$ ) provided a value of  $x = 0.24 \pm 0.05$ , the majority of the quoted error being due to the absolute uncertainties in the reference spectra. Thus, a value of  $\alpha_{13} = 0.61 \pm 0.07$  is obtained.

Since the secondary chemistry following reaction (13) leads to further removal of  $CH_2=CHCH_2O_2$  [reaction sequence (14) + (15)], the observed second-order rate coefficient,  $k_{13obs}$ , presented in the preceding section, is greater than the elementary coefficient,  $k_{13}$ , as discussed in detail previously for other organic peroxy radicals.<sup>3</sup> Provided reaction (15) is predominant for  $HO_2$ , the observed and elementary coefficients are related by the simple expression  $k_{13obs} = (1 + \alpha_{13})k_{13}$ . With this assumption, the value of  $k_{13} = (6.8 \pm 1.3) \times 10^{-13}$   $cm^3$  molecule<sup>-1</sup> s<sup>-1</sup> may be calculated.

The sensitivity of the system to variation of  $[O_2]$  was investigated. The time dependences of the accumulation of  $CH_2=CHCHO$  and  $CH_2=CHCH_2OH$  in experiments performed with  $[O_2] = 2.4 \times 10^{19}$ ,  $3.7 \times 10^{18}$  and  $1.3 \times 10^{17}$  molecule  $cm^{-3}$ , for similar initial allyl iodide concentrations are shown in Fig. 11. As  $[O_2]$  was decreased, the yield of  $CH_2=CHCHO$  relative to allyl iodide lost also decreased, implying the existence of a reaction competing with the reaction of  $CH_2=CHCH_2O$  with  $O_2$  [reaction (14)]. The thermal decomposition reaction (16), producing HCHO and  $CH_2=CH$ , is one possible candidate. However, although HCHO was detected in trace amounts at the lower  $[O_2]$  (ca. 1% of  $[CH_2=CHCHO]$ ), the concentrations were insufficient to be accounted for by reaction (16) becoming competitive. Furthermore, the reduction in the  $CH_2=CHCHO$  yield

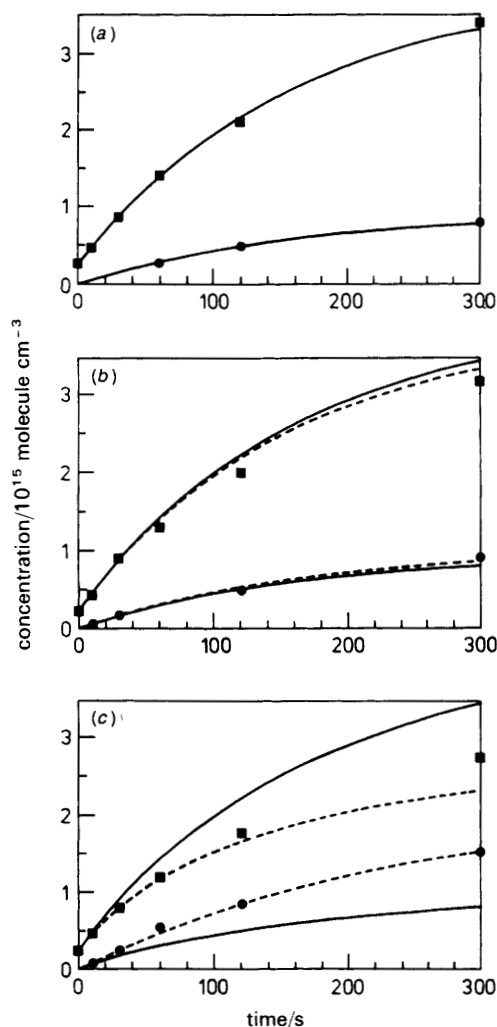
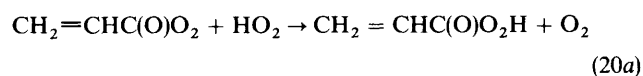
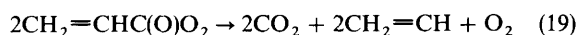
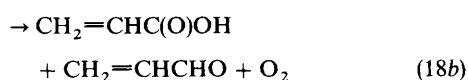
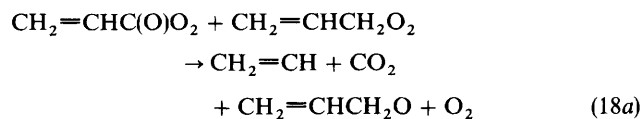


**Fig. 11** Plots of accumulation of  $CH_2=CHCHO$  (■) and  $CH_2=CHCH_2OH$  (●) as a function of  $[O_2]$  during the 253.7 nm photolysis of allyl iodide- $O_2$  mixtures. (a)  $[O_2] = 2.4 \times 10^{19}$ ; (b)  $[O_2] = 3.7 \times 10^{18}$ ; and (c)  $[O_2] = 1.3 \times 10^{17}$  molecule  $cm^{-3}$ . Lines are results of simulations (see text)

at lower  $[O_2]$  was accompanied by a comparable increase in the yield of  $CH_2=CHCH_2OH$  (see Fig. 11). This suggests that  $CH_2=CHCH_2O$  might abstract the labile, aldehydic hydrogen atom from  $CH_2=CHCHO$  to produce  $CH_2=CHCH_2OH$  directly:



Although this reaction provides a plausible explanation for the observed  $O_2$  effect, its precise influence may only be assessed if the chemistry of the acyl radical  $CH_2=CHCO$  formed simultaneously with  $CH_2=CHCH_2OH$  is known. Initial combination with  $O_2$  to produce the peroxy radical  $CH_2=CHC(O)O_2$  is most likely, and this will react with the other peroxy radicals present as follows:



Clearly, the situation is complex, since both  $CH_2=CHCHO$  and  $CH_2=CHCH_2O$  are regenerated by these reactions, and the relative rates of the reactions are not known. Reactions (18a) and (19) produce the vinyl radical,  $CH_2=CH$ , the oxidation of which can explain the observation of low concentrations of  $HCHO$ .<sup>19,20</sup> Other residual absorptions observed at low  $[O_2]$ , particularly in the carbonyl region, may be due to  $CH_2=CHC(O)OH$  or  $CH_2=CHC(O)O_2H$ .

The accumulation rate of  $CH_2=CHCHO$  and  $CH_2=CHCH_2OH$  was simulated using the chemical mechanism listed in Table 5. Fig. 11 shows the results of simula-

tions compared with the experimental data obtained at the three  $O_2$  concentrations. The continuous lines are the results of simulations using the elementary mechanism not incorporating reaction (17) and the subsequent chemistry. Clearly this is only adequate to describe the high  $[O_2]$  data. The broken lines demonstrate the effect of including the additional chemistry [reactions (18)–(20)], initiated by reaction (17), with estimated rate coefficients as given in Table 5. Since the calculated yield of  $CH_2=CHCH_2OH$  is less sensitive than the yield of  $CH_2=CHCHO$  to errors in the estimated rate coefficients, an optimised value of  $k_{17}/k_{14}$  was obtained by fitting only to the  $CH_2=CHCH_2OH$  yields in the intermediate and low  $[O_2]$  experiments. However, the time dependence of  $CH_2=CHCHO$  is also reasonably well described with the parameters chosen. The optimised value of  $k_{17}/k_{14}$  was 55. Assuming reaction (14) has a rate coefficient comparable with those observed for simple alkoxy radicals (*ca.*  $7 \times 10^{-15} \text{ cm}^3 \text{ molecule}^{-1} \text{ s}^{-1}$ ), a value of  $k_{17} \approx 4 \times 10^{-13} \text{ cm}^3 \text{ molecule}^{-1} \text{ s}^{-1}$  is calculated.

## Discussion

### UV Absorption Spectrum and Kinetics of Reactions of $CH_2=CHCH_2$

The experiments on the flash photolysis of hexa-1,5-diene- $N_2$  and allyl iodide- $N_2$  mixtures allowed absolute determination of the low-resolution spectrum of  $CH_2=CHCH_2$  over the wavelength range 210–232.5 nm. The spectral shape was determined from experiments in which hexa-1,5-diene was photolysed using 193 nm radiation. Absolute calibration was achieved by using the 248 nm photolysis of allyl iodide as an alternative source, the  $CH_2=CHCH_2$  cross-sections being calibrated relative to the loss of allyl iodide with the assumption that C–I bond fission was the exclusive photolysis pathway:



The results of the FTIR product study of the 253.7 nm photolysis of allyl iodide support this assumption, since the observed organic products are those expected from the oxidation of  $CH_2=CHCH_2$ , and their yields balance the loss of

Table 5 Reactions and rate coefficients used to simulate the photo-oxidation of allyl iodide

reaction	rate coefficient <sup>a</sup>
standard mechanism	
$CH_2=CHCH_2I + h\nu \rightarrow CH_2=CHCH_2 + I$	$6.3 \times 10^{-3} \text{ s}^{-1} \text{ }^b$
$CH_2=CHCH_2 + O_2(+M) \rightarrow CH_2=CHCH_2O_2(+M)$	$6.0 \times 10^{-13} \text{ }^b$
$I + I(+M) \rightarrow I_2(+M)$	$(2.5\text{--}5.0) \times 10^{-13} \text{ }^c$
$CH_2=CHCH_2 + I_2 \rightarrow CH_2=CHCH_2I + I$	$1.2 \times 10^{-11} \text{ }^b$
$2CH_2=CHCH_2O_2 \rightarrow 2CH_2=CHCH_2O + O_2$	$4.1 \times 10^{-13} \text{ }^b$
$\rightarrow CH_2=CHCHO + CH_2=CHCH_2OH + O_2$	$2.7 \times 10^{-13} \text{ }^b$
$CH_2=CHCH_2O + O_2 \rightarrow CH_2=CHCHO + HO_2$	$7.0 \times 10^{-15} \text{ }^d$
$CH_2=CHCH_2O_2 + HO_2 \rightarrow CH_2=CHCH_2O_2H + O_2$	$1.0 \times 10^{-11} \text{ }^d$
$HO_2 + HO_2 \rightarrow H_2O_2 + O_2$	$(2.70\text{--}2.85) \times 10^{-12} \text{ }^e$
additional chemistry	
$CH_2=CHCH_2O + CH_2=CHCHO \rightarrow CH_2=CHCH_2OH + CH_2=CHCO$	varied (see text)
$CH_2=CHCO + O_2 + M \rightarrow CH_2=CHC(O)O_2 + M$	$5.0 \times 10^{-12} \text{ }^f$
$2CH_2=CHC(O)O_2 \rightarrow 2CH_2=CH + 2CO_2 + O_2$	$1.7 \times 10^{-11} \text{ }^f$
$CH_2=CHC(O)O_2 + CH_2=CHCH_2O_2 \rightarrow CH_2=CH + CO_2 + CH_2=CHCH_2O + O_2$	$6.5 \times 10^{-12} \text{ }^f$
$\rightarrow CH_2=CHCHO + CH_2=CHC(O)OH + O_2$	$6.5 \times 10^{-12} \text{ }^f$
$CH_2=CHC(O)O_2 + HO_2 \rightarrow CH_2=CHC(O)O_2H + O_2$	$1.0 \times 10^{-11} \text{ }^f$
$\rightarrow CH_2=CHC(O)OH + O_3$	$4.0 \times 10^{-12} \text{ }^f$
$CH_2=CH + O_2 \rightarrow HCHO + HCO$	$1.0 \times 10^{-11} \text{ }^g$
$HCO + O_2 \rightarrow HO_2 + CO$	$5.6 \times 10^{-12} \text{ }^h$

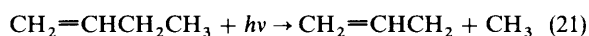
<sup>a</sup> Units  $\text{cm}^3 \text{ molecule}^{-1} \text{ s}^{-1}$  unless otherwise stated. <sup>b</sup> Taken from the present study. <sup>c</sup> Rate coefficient varies as a function of  $[O_2]$ . Values taken from ref. 18. The real recombination rate will probably be significantly more rapid owing to catalysis by the presence of  $RO_2$ . However, even with the parameters used, recombination occurs on the timescale of *ca.* 1 s. <sup>d</sup> Estimated. <sup>e</sup> Rate coefficient varies as a function of  $[O_2]$ . Values taken from ref. 21. <sup>f</sup> Estimated by comparison with rate coefficients of analogous reactions involving  $CH_3C(O)O_2$ , as given in ref. 21. <sup>g</sup> Taken from ref. 20. <sup>h</sup> Taken from ref. 21.

allyl iodide, within experimental error. Furthermore, no strong evidence was obtained for the formation of allene,  $\text{CH}_2=\text{C}=\text{CH}_2$ , or HI which would result from the possible alternative photolysis pathway:



In experiments performed with high allyl iodide concentrations (*ca.*  $2 \times 10^{16}$  molecule  $\text{cm}^{-3}$ ) trace residual features were observed at *ca.* 1920 and 850  $\text{cm}^{-1}$  which may be due to  $\text{CH}_2=\text{C}=\text{CH}_2$ . With this attribution, it is concluded that channel (6a) accounts for  $\leq 1\%$  of the removal of allyl iodide during photolysis at 253.7 nm.

The resultant absorption cross-section near the maximum,  $\sigma(220 \text{ nm}) = (5.8 \pm 0.8) \times 10^{-17}$   $\text{cm}^2$  molecule $^{-1}$  agrees well with the value determined by Van den Bergh and Callear<sup>13</sup> at the same wavelength,  $\sigma(220 \text{ nm}) = 5.4 \times 10^{-17}$   $\text{cm}^2$  molecule $^{-1}$ . Van den Bergh and Callear calibrated the  $\text{CH}_2=\text{CHCH}_2$  spectrum relative to that of  $\text{CH}_3$ , by assuming that the flash photolysis of but-1-ene at low flash energies generated equal quantities of the two radicals:



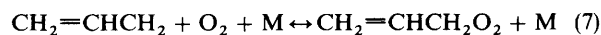
In view of the quantitative agreement with the present determination, this assumption seems justified. The absorption cross-sections measured at 2.5 nm intervals in the present study are compared with the higher resolution spectrum of Van den Bergh and Callear in Fig. 6. In both cases, the relative spectrum was determined from experiments involving the flash photolysis of hexa-1,5-diene. Clearly, the agreement is very good over the complete wavelength range.

There have been two previous determinations of  $k_{10}/\sigma$ , both measured at 223 nm, which differ by a factor of almost 2. Van den Bergh and Callear obtained a value of  $(2.5 \pm 0.9) \times 10^5$   $\text{cm s}^{-1}$ , whereas Tulloch *et al.*<sup>14</sup> reported a value of  $(4.60 \pm 0.35) \times 10^5$   $\text{cm s}^{-1}$ . The present determination at 222.5 nm,  $(4.82 \pm 0.55) \times 10^5$   $\text{cm s}^{-1}$ , clearly confirms the value of Tulloch *et al.*, with both measurements made using the 193 nm laser photolysis of hexa-1,5-diene as the source of  $\text{CH}_2=\text{CHCH}_2$ . Although Van den Bergh and Callear also used hexa-1,5-diene as the precursor, photolysis was achieved using flash lamps emitting over the wavelength range 185–205 nm. They reported a small contribution at 216 nm due to the presence of  $\text{CH}_3$  in the initial radical population, which also implies the existence of one or more isomeric  $\text{C}_5\text{H}_7$  radicals, formed simultaneously from the minor photolysis channel:



The product study of Tulloch *et al.* suggests  $\text{CH}_3$  and  $\text{C}_5\text{H}_7$  will each be present at only *ca.* 2% of the concentration of  $\text{CH}_2=\text{CHCH}_2$  following 193 nm photolysis of hexa-1,5-diene. If a significantly greater relative concentration of these radicals was generated by the broad-band photolysis, then some complication in the determinations of  $k_{10}/\sigma(223 \text{ nm})$  might result.

The value of  $k_7 = (6 \pm 2) \times 10^{-13}$   $\text{cm}^3$  molecule $^{-1}$   $\text{s}^{-1}$  is about an order of magnitude lower than the high pressure limiting rate coefficients typically observed for the reactions of simple alkyl radicals with  $\text{O}_2$  at room temperature:



Reaction (7) has previously been studied in some detail by Morgan *et al.*<sup>15</sup> over the temperature range 382–453 K, at 50 Torr total pressure. Significant curvature was observed in the Arrhenius plot of  $k_7$ , and a less extensive study of the pressure dependence indicated that the reaction was in the fall-off region at the high end of the temperature range. At the lowest temperatures investigated,  $k_7$  was varying only weakly with

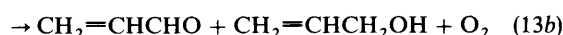
temperature and a value of *ca.*  $4 \times 10^{-13}$   $\text{cm}^3$  molecule $^{-1}$   $\text{s}^{-1}$  was observed, consistent with the value obtained from the present experiments. The back decomposition of  $\text{CH}_2=\text{CHCH}_2\text{O}_2$  [reaction (–7)] was found to be important at these elevated temperatures, with  $k_{-7}$  described by the expression  $1.6 \times 10^{10} \exp(-6411/T)$   $\text{s}^{-1}$ . Thus at 296 K, the back decomposition rate extrapolated using this expression is *ca.* 6  $\text{s}^{-1}$ , which is negligibly slow on the timescale of the measurements of the forward rate coefficient (0.2 ms) in the present study.

There are no reported determinations of the rate coefficient for the reaction of  $\text{CH}_2=\text{CHCH}_2$  with I atoms [reaction (12)], which explains the rapid removal of  $\text{CH}_2=\text{CHCH}_2$  following the 248 nm photolysis of allyl iodide observed in the present study. The value of  $k_{12} = (1.6 \pm 0.6) \times 10^{-10}$   $\text{cm}^3$  molecule $^{-1}$   $\text{s}^{-1}$ , is significantly greater than published rate coefficients for reactions of perfluorinated alkyl radicals with I atoms<sup>22</sup> ( $\text{CF}_3$ ,  $\text{C}_2\text{F}_5$ ,  $\text{C}_3\text{F}_7$ ,  $\text{C}_4\text{F}_9$ ), which lie in the range  $(0.85\text{--}2.3) \times 10^{-11}$   $\text{cm}^3$  molecule $^{-1}$   $\text{s}^{-1}$  at 298 K. Similarly, there are no reported measurements of the rate of the reactions of  $\text{CH}_2=\text{CHCH}_2$  with  $\text{I}_2$  [reaction (11)]. The FTIR study of the photolysis of allyl iodide allowed the rate of this reaction to be measured relative to reaction (7). The value of  $k_{11}/k_7$  obtained,  $(20 \pm 7)$ , implies a value of  $k_{11} = (1.2 \pm 0.6) \times 10^{-11}$   $\text{cm}^3$  molecule $^{-1}$   $\text{s}^{-1}$ , based on the value of  $k_7$  measured in the present work. This is comparable to a range of reported measurements for reactions of alkyl radicals with  $\text{I}_2$ <sup>22</sup> which, although subject to some scatter, appear to lie in the range  $10^{-12}\text{--}10^{-11}$   $\text{cm}^3$  molecule $^{-1}$   $\text{s}^{-1}$ .

#### UV Absorption spectrum and Self-reaction of $\text{CH}_2=\text{CHCH}_2\text{O}_2$

The broad-band absorption spectrum observed from the 193 nm flash photolysis of hexa-1,5-diene- $\text{O}_2$  mixtures is attributed to  $\text{CH}_2=\text{CHCH}_2\text{O}_2$  formed from reaction (7). The spectrum is typical of an organic peroxy radical, with the maximum observed at 235 nm (see Fig. 6). Comparison with the single reported spectrum of the corresponding saturated alkyl peroxy radical,  $\text{CH}_3\text{CH}_2\text{CH}_2\text{O}_2$ ,<sup>3,23</sup> indicates that the  $\text{CH}_2=\text{CHCH}_2\text{O}_2$  spectrum is similar in shape, but shifted to shorter wavelength by *ca.* 5–10 nm. The absolute cross-sections were calibrated relative to those determined for  $\text{CH}_2=\text{CHCH}_2$  in the absence of  $\text{O}_2$ , and are believed to be accurate to  $\pm 15\%$ . The maximum cross-section,  $\sigma(235 \text{ nm}) = 6.2 \times 10^{-18}$   $\text{cm}^2$  molecule $^{-1}$ , is therefore comparable with that observed for  $\text{CH}_3\text{CH}_2\text{CH}_2\text{O}_2$ ,  $\sigma(240 \text{ nm}) = 4.2 \times 10^{-18}$   $\text{cm}^2$  molecule $^{-1}$ , within the combined experimental errors.

The removal of  $\text{CH}_2=\text{CHCH}_2\text{O}_2$  was initiated by the self-reaction (13), with an observed rate coefficient  $k_{13\text{obs}} = (1.1 \pm 0.2) \times 10^{-12}$   $\text{cm}^3$  molecule $^{-1}$   $\text{s}^{-1}$ , which is about a factor of 3 greater than that reported for  $\text{CH}_3\text{CH}_2\text{CH}_2\text{O}_2$ :



The value of  $\alpha_{13} = (0.61 \pm 0.07)$  determined from the FTIR product analysis allowed correction for the secondary removal of  $\text{CH}_2=\text{CHCH}_2\text{O}_2$  by reaction sequence (14) + (15), and an elementary rate coefficient  $k_{13} = (6.8 \pm 1.3) \times 10^{-13}$   $\text{cm}^3$  molecule $^{-1}$   $\text{s}^{-1}$  was derived:



The present determination of  $\alpha_{13}$  further supports the conclusion that the relative importance of the terminating and propagating channels, analogous to (13b) and (13a) for a range of  $\text{RO}_2$  radicals at ambient temperatures, is remarkably insensitive to the nature of R, even though the overall rate coefficients differ by several orders of magnitude (see Lightfoot *et al.*<sup>3</sup>). Indeed, reported values of  $\alpha$  for the alkyl or substituted alkyl peroxy radicals  $\text{C}_2\text{H}_5\text{O}_2$ ,<sup>3</sup>  $\text{ClCH}_2\text{CH}_2\text{O}_2$ <sup>3,24</sup> and  $\text{BrCH}_2\text{CH}_2\text{O}_2$ <sup>25</sup> lie in the range 0.6–0.7 (*i.e.* identical to that measured for  $\text{CH}_2=\text{CHCH}_2\text{O}_2$ ), despite a factor of 60 range in the rate coefficients.<sup>3,26,27</sup> One exception to the rule is  $\text{HOCH}_2\text{CH}_2\text{O}_2$ , for which the reported value of  $\alpha$  is 0.36.<sup>3,12</sup> This may result from a degree of internal hydrogen bonding in this radical.

The FTIR product study established that the alkoxy radical,  $\text{CH}_2=\text{CHCH}_2\text{O}$ , formed from the self-reaction of the peroxy radical, reacts predominantly with  $\text{O}_2$  [reaction (14)]. There was no evidence for the potential competing thermal decomposition reaction:



Thus under atmospheric conditions,  $\text{CH}_2=\text{CHCH}_2\text{O}$  and other alkoxy-type radicals are predicted to react with  $\text{O}_2$  in preference to decomposition to yield vinyl-type radicals. Under the conditions of the product study, however, there was evidence for a competing reaction which gained importance as the  $\text{O}_2$  concentration was lowered, or the initial allyl iodide concentration was raised, which is believed to be the reaction of  $\text{CH}_2=\text{CHCH}_2\text{O}$  with the product  $\text{CH}_2=\text{CHCHO}$ :



This conclusion was based primarily on the reduction in the yield of  $\text{CH}_2=\text{CHCHO}$  at longer photolysis times in the low  $[\text{O}_2]$  or high [allyl iodide] experiments being accompanied by a comparable increase in the yield of  $\text{CH}_2=\text{CHCH}_2\text{OH}$ . Simulation of the observed product–time curves (Fig. 11) provided a value of  $k_{17}/k_{14} \approx 55$ . Evidence for a similar H-atom abstraction reaction for  $\text{CH}_3\text{O}$  was found previously by Moortgat *et al.*<sup>28</sup> during their study of the photo-oxidation of  $\text{CH}_3\text{CHO}$ . On the basis of the observed yields of  $\text{CH}_3\text{OH}$ , they concluded that a competition existed between reactions (22) and (23), and a value of  $k_{23}/k_{22} \approx 115$  was derived from computer simulation of the system:



These results strongly suggest that RO radicals derived from hydrocarbons are able to abstract labile hydrogen atoms such as those found in aldehydes, with rate coefficients of the order of  $10^{-13} \text{ cm}^3 \text{ molecule}^{-1} \text{ s}^{-1}$ .

### Application to the Oxidation of Isoprene in the Planetary Boundary Layer

Numerous studies in recent years have established the presence of significant concentrations of non-methane hydrocarbons of biogenic origin in the planetary boundary layer above remote forested regions.<sup>5–10</sup> In particular, isoprene is typically observed at levels in excess of 1 ppbv. Since its reaction with OH radicals is rapid ( $1.01 \times 10^{-10} \text{ cm}^3 \text{ molecule}^{-1} \text{ s}^{-1}$ ) isoprene at these mixing ratios provides a major sink for OH. Although several studies of the end products of isoprene oxidation at high [NO] have been published,<sup>29–32</sup> little is known about the elementary reactions in the detailed degra-

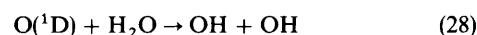
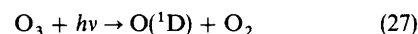
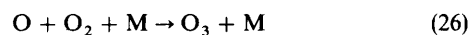
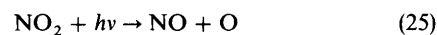
ation mechanism. The allyl/ $\beta$ -hydroxy peroxy radicals ( $\text{RO}_2$ ) formed following the addition of OH to isoprene (see Fig. 1), are likely to have several reactions available under tropospheric conditions. If  $\text{NO}_x$  levels are high enough, the reactions of  $\text{RO}_2$  with NO will dominate, leading mainly to the production of the alkoxy radical RO:



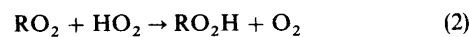
The available information indicates that the subsequent reactions of the RO radicals are propagating, leading to the generation of oxygenated products such as methacrolein [ $\text{CH}_2=\text{C}(\text{CH}_3)\text{CHO}$ ], methyl vinyl ketone [ $\text{CH}_3\text{C}(\text{O})\text{CH}=\text{CH}_2$ ] and HCHO, but also producing  $\text{HO}_2$ , which leads to the regeneration of OH:



Consequently, if reaction (1) is dominant for  $\text{RO}_2$ , OH is not lost, since its rate of regeneration by reaction (24) balances its removal rate by reaction with isoprene. Furthermore, the concurrent generation of  $\text{NO}_2$  in reactions (1) and (24) results in the production of  $\text{O}_3$ , following the photolysis of  $\text{NO}_2$ , and this in turn promotes further OH production:



At lower levels of  $\text{NO}_x$ , the reactions of  $\text{RO}_2$  with itself and other peroxy radicals ( $\text{R}'\text{O}_2$  or  $\text{HO}_2$ ) are able to compete with reaction (1):



On the basis of available data, reaction (2) will be entirely terminating.<sup>3</sup> The results of the present study for  $\text{CH}_2=\text{CHCH}_2\text{O}_2$ , and the previous work on  $\text{HOCH}_2\text{CH}_2\text{O}_2$ ,<sup>11,12</sup> indicate that reactions (3) and (4) will be significantly terminating. Consequently, at low levels of  $\text{NO}_x$ , the presence of isoprene (and monoterpenes) may have a dramatic effect on the boundary layer radical population, in particular on the concentration of OH.

If the relative rate coefficients for the competing  $\text{RO}_2$  radical reactions (1)–(4) can be estimated, it is possible to assess the influence of elevated concentrations of isoprene on the radical population ( $\text{OH}$ ,  $\text{HO}_2$ ,  $\text{RO}_2$ ), and on the  $\text{O}_3$  and  $\text{NO}_x$  chemistry. The present study and our previous work,<sup>11,12</sup> indicate that the allyl functionality has an activating influence on the peroxy radical self-reaction rate, and the  $\beta$ -hydroxy group activates both the self-reaction of the peroxy radical, and its reaction with  $\text{HO}_2$ . Consequently, the  $\text{RO}_2$  radicals derived from isoprene and other unsaturated biogenic compounds will probably react rapidly with peroxy radicals in general (*i.e.*  $\text{RO}_2$ ,  $\text{R}'\text{O}_2$  or  $\text{HO}_2$ ). In contrast, the reaction of  $\text{HOCH}_2\text{CH}_2\text{O}_2$  with NO has been found to proceed at a comparable rate to the reaction of the unsubstituted counterpart,  $\text{C}_2\text{H}_5\text{O}_2$ , with NO.<sup>3,33</sup>

Rate coefficients for reactions of the  $\text{RO}_2$  radicals derived from isoprene have been estimated, as shown in Table 6. The  $\text{RO}_2$  species have all been assigned the same rate coefficients and therefore behave indistinguishably. Thus, in the following discussion, ' $\text{RO}_2$ ' implies total organic peroxy radical population (excluding  $\text{CH}_3\text{O}_2$ ), and the  $\text{RO}_2$  self-reaction incorporates all the mutual reactions of the peroxy radical species

**Table 6** Rate coefficients used to model the behaviour of radical species in the OH-initiated oxidation of isoprene

reaction	rate coefficient /cm <sup>3</sup> molecule <sup>-1</sup> s <sup>-1</sup>
OH + isoprene (+ O <sub>2</sub> ) → RO <sub>2</sub>	1.0 × 10 <sup>-10</sup> <sup>a</sup>
RO <sub>2</sub> + RO <sub>2</sub> → HO <sub>2</sub> + HO <sub>2</sub>	5.9 × 10 <sup>-13</sup> <sup>b</sup>
→ stable products	6.3 × 10 <sup>-13</sup> <sup>b</sup>
RO <sub>2</sub> + HO <sub>2</sub> → stable products	1.0 × 10 <sup>-11</sup> <sup>c</sup>
RO <sub>2</sub> + CH <sub>3</sub> O <sub>2</sub> → HO <sub>2</sub> + HO <sub>2</sub>	2.7 × 10 <sup>-13</sup> <sup>d</sup>
→ stable products	4.0 × 10 <sup>-13</sup> <sup>d</sup>
RO <sub>2</sub> + NO → HO <sub>2</sub> + NO <sub>2</sub>	8.1 × 10 <sup>-12</sup> <sup>e</sup>
→ RONO <sub>2</sub>	9.0 × 10 <sup>-13</sup> <sup>e</sup>
O <sub>3</sub> + isoprene → stable products	1.4 × 10 <sup>-17</sup> <sup>f</sup>
→ RO <sub>2</sub>	

<sup>a</sup> Taken from ref. 34. <sup>b</sup> Overall rate coefficient is geometric mean of and branching ratio is the arithmetic mean of those observed for CH<sub>2</sub>=CHCH<sub>2</sub>O<sub>2</sub> and HOCH<sub>2</sub>CH<sub>2</sub>O<sub>2</sub> (ref. 3). <sup>c</sup> Equivalent to the recommended rate coefficient for HOCH<sub>2</sub>CH<sub>2</sub>O<sub>2</sub> (ref. 3). <sup>d</sup> Overall rate coefficient is geometric mean and branching ratio is the arithmetic mean of those used above for self-reaction of RO<sub>2</sub>, and those recommended for self-reaction of CH<sub>3</sub>O<sub>2</sub> (ref. 3). <sup>e</sup> Overall rate coefficient is that published for HOCH<sub>2</sub>CH<sub>2</sub>O<sub>2</sub> (ref. 3 and 33). Branching ratio is that reported for isoprene in ref. 3. <sup>f</sup> Rate coefficient taken from ref. 2 and applied to either channel as discussed in the text.

(i.e. RO<sub>2</sub> + R'O<sub>2</sub>). The reactions displayed in the table have been incorporated into a simple boundary layer box model described previously<sup>35</sup> in order to assess the impact of 3 ppbv of isoprene on levels of OH, HO<sub>2</sub>, RO<sub>2</sub> and O<sub>3</sub> as a function of [NO<sub>x</sub>]. The background chemistry incorporates the chemical transformations occurring in the oxidation of CO and CH<sub>4</sub>, which are present at fixed levels of 150 ppbv and 1.7 ppmv, respectively. The complete background chemical scheme is given in ref. 35. The model is intended to represent a well mixed boundary layer air mass which is isolated from the background troposphere for a characteristic period of one day. The steady-state concentrations of the range of species are determined for conditions appropriate to 40°-N (equinox) using averaged daytime photodissociation constants, but no attempt is made to investigate diurnal variations.

The calculated steady-state concentrations of the radical species and O<sub>3</sub> are shown as a function of [NO<sub>x</sub>] in Fig. 12 and 13. The reference level of 20 ppbv O<sub>3</sub> is the concentration which would be present in the absence of the chemistry, due to the mixing in of air from the background troposphere. Certain observations can be drawn:

(i) At low [NO<sub>x</sub>] (<40 pptv) the calculated concentration of OH is ca. (1–2) × 10<sup>5</sup> molecule cm<sup>-3</sup> (see Fig. 12). This is about an order of magnitude lower than that calculated for similar conditions in the absence of isoprene.<sup>35</sup> The concentration of OH is significantly suppressed by the rapid reaction with isoprene, since reaction (1) leading to OH regeneration is unable to compete with RO<sub>2</sub> removal by its self-reactions. High levels of RO<sub>2</sub> are observed (ca. 5 × 10<sup>8</sup> molecule cm<sup>-3</sup>), since the concentration is only controlled by the self-reactions. Small O<sub>3</sub> depletions result from the removal of the radical species [reactions (2) and (3)], which are generated from O<sub>3</sub> photolysis.

(ii) At intermediate [NO<sub>x</sub>] (40 pptv < [NO<sub>x</sub>] < 4 ppbv), significant regeneration of OH occurs as a result of reaction (1) becoming progressively more dominant for RO<sub>2</sub>. [OH] increases with [NO<sub>x</sub>] up to a peak of ca. 10<sup>6</sup> molecule cm<sup>-3</sup>, and substantial O<sub>3</sub> formation is calculated (Fig. 13). However, OH concentrations are still approaching an order of magnitude lower than those calculated for comparable scenarios in the absence of isoprene.<sup>35</sup>

(iii) At high [NO<sub>x</sub>] (>4 ppbv) efficient removal of OH by reaction with NO<sub>2</sub> results in a dramatic reduction in the con-

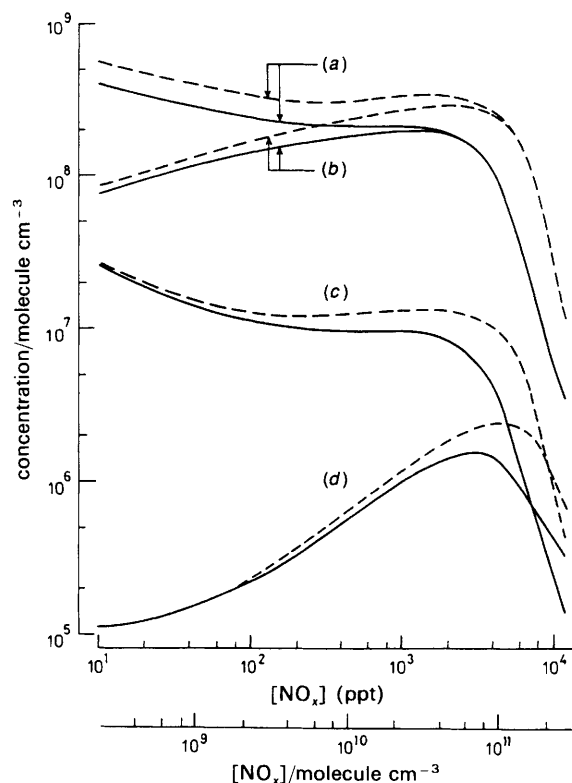


**Fig. 12** Calculated steady-state concentrations of (a) RO<sub>2</sub>, (b) HO<sub>2</sub>, (c) CH<sub>3</sub>O<sub>2</sub> and (d) OH as a function of [NO<sub>x</sub>]. Solid lines, O<sub>3</sub> + isoprene reaction assumed to lead to no radical production. Broken lines, O<sub>3</sub> + isoprene reaction assumed to lead to RO<sub>2</sub> production

centration of all the radical species (Fig. 12):



Since this inhibits the O<sub>3</sub> production mechanism, a dramatic decrease in [O<sub>3</sub>] is also calculated.

It should be noted that the above calculations were performed for a constant isoprene concentration of 3 ppbv independent of [NO<sub>x</sub>]. This is somewhat artificial since the removal rate of isoprene will be greater at higher [OH], so its concentration is more likely to be suppressed in the intermediate [NO<sub>x</sub>] range, with the oxidation products accumulating more rapidly, and competing for OH. Nevertheless, the simplified calculations have allowed some interesting observations to be made.

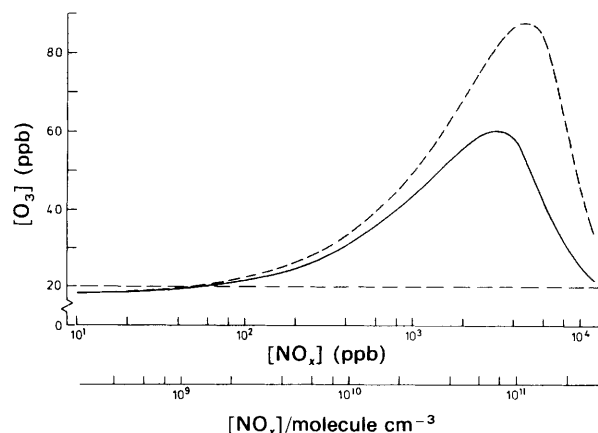
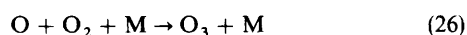
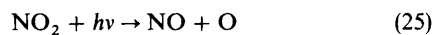
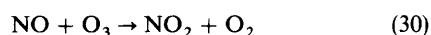


**Fig. 13** Calculated O<sub>3</sub> concentrations as a function of [NO<sub>x</sub>]. Solid line, O<sub>3</sub> + isoprene reaction assumed to lead to no radical production. Broken line, O<sub>3</sub> + isoprene reaction assumed to lead to RO<sub>2</sub> production. The horizontal broken line is the 20 ppbv reference level of O<sub>3</sub>

The discussion so far has concentrated mainly on the influence of  $\text{NO}_x$  on the chemistry of  $\text{RO}_2$ . Conversely, the high concentrations of  $\text{RO}_2$  and  $\text{HO}_2$  generated are able to influence the partition of the  $\text{NO}_x$  species by perturbing their interconversion chemistry. Under most scenarios appropriate to the troposphere the interconversion of  $\text{NO}$  and  $\text{NO}_2$  by the following 'null cycle' determines the relative concentration of the two species,<sup>3,35</sup> (i.e.  $k_{30}[\text{NO}][\text{O}_3]/J_{25}[\text{NO}_2] = 1$ : the photostationary-state condition):



The presence of high concentrations of  $\text{RO}_2$  and  $\text{HO}_2$  provides additional  $\text{NO}$  to  $\text{NO}_2$  conversion routes which compete with reaction (30), and deviations from the photostationary state condition are calculated (see Fig. 14):



Owing to the suppression of  $[\text{OH}]$  over the complete range of conditions considered the oxidation of isoprene will be initiated at a comparable rate by reaction with  $\text{O}_3$ . This does not necessarily represent a sink for  $\text{O}_3$ , however, since available information indicates that the reaction of  $\text{O}_3$  with isoprene leads to significant formation of radical products,<sup>36,37</sup> with the subsequent generation of  $\text{O}_3$ . In order to demonstrate the influence of this reaction, calculations were performed with the reaction either exclusively terminating, or generating one  $\text{RO}_2$  per  $\text{O}_3$ -isoprene reaction. As can be seen from Fig. 12-14, the influence of this reaction on the observed concentrations of  $\text{OH}$ ,  $\text{HO}_2$ ,  $\text{RO}_2$ ,  $\text{O}_3$  and  $\text{NO}_x$  is strongly dependent on the extent to which it generates radical products.

Another potentially important species for initiating the oxidation of isoprene and monoterpenes is the  $\text{NO}_3$  radical.<sup>38</sup> However, tabulations of comparative terpene lifetimes with respect to reaction with  $\text{OH}$ ,  $\text{O}_3$  and  $\text{NO}_3$  usually assume

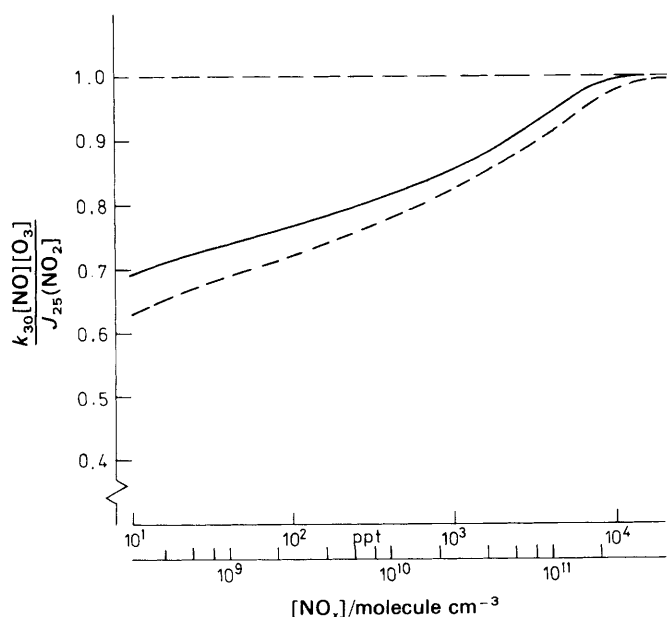


Fig. 14 Deviations from  $\text{NO}_x$  photostationary-state condition calculated as a function of  $[\text{NO}_x]$ . Solid line,  $\text{O}_3$  + isoprene reaction assumed to lead to no radical production. Broken line,  $\text{O}_3$  + isoprene reaction assumed to lead to  $\text{RO}_2$  production

'typical' concentrations of these species, for which  $[\text{NO}_3] = 10$  pptv (ca.  $2.5 \times 10^8$  molecule  $\text{cm}^{-3}$ ) is often adopted. Although this may be appropriate for some scenarios it should be noted that for elevated concentrations of isoprene and terpenes, this figure is inappropriate since  $\text{NO}_3$  initiates, but does not catalyse, the degradation, so the reactions with the terpenes may dramatically suppress its concentration, as discussed previously by Winer *et al.*<sup>39</sup> For example, at 1 ppbv  $\text{NO}_2$  and 30 ppbv  $\text{O}_3$ , 3 ppbv isoprene will limit the concentration of  $\text{NO}_3$  to ca. 0.5 pptv ( $1.3 \times 10^7$  molecule  $\text{cm}^{-3}$ ). The monoterpenes are generally even more reactive towards  $\text{NO}_3$ , and greater suppression of  $[\text{NO}_3]$  would occur in the presence of ppbv levels of these species. Clearly, under many conditions, reactive biogenic hydrocarbons provide an efficient sink for  $\text{NO}_3$ , but not *vice versa*.

We gratefully acknowledge support for this work provided by the Commission of the European Communities (under contract EV4V-0082-C), the Natural Environment Research Council (Marine and Atmospheric Sciences Division) and the UK Department of the Environment (under contract PECD 7/10/147). Dr F. Danis is thanked for his assistance in the construction of the laser photolysis apparatus.

## References

- 1 J. G. Calvert and S. Madronich, *J. Geophys. Res.*, 1987, **92**, 2211.
- 2 R. Atkinson, *Atmos. Environ. A*, 1990, **24**, 1.
- 3 P. D. Lightfoot, R. A. Cox, J. N. Crowley, M. Destriau, G. D. Hayman, M. E. Jenkin, G. K. Moortgat and F. Zabel, *Atmos. Environ. A*, 1992, **26**, 1805.
- 4 T. J. Wallington, P. Dagaut and M. J. Kurylo, *Chem. Rev.*, 1992, **92**, 667.
- 5 J. P. Greenberg and P. R. Zimmerman, *J. Geophys. Res.*, 1984, **89**, 4667.
- 6 P. J. Crutzen, A. C. Delany, J. P. Greenberg, P. Haagenson, L. Heidt, R. Lueb, W. Pollock, W. Seiler, A. Wartburg and P. R. Zimmerman, *J. Atmos. Chem.*, 1985, **2**, 233.
- 7 G. L. Gregory, R. C. Harriss, R. W. Talbot, R. A. Rasmussen, M. Garstang, M. O. Andreae, R. R. Hinton, E. V. Browell, S. M. Beck, D. I. Sebacher, M. A. K. Khalil, R. J. Ferek and S. V. Harriss, *J. Geophys. Res.*, 1986, **91**, 8603.
- 8 P. L. Zimmerman, J. P. Greenberg and C. E. Westberg, *J. Geophys. Res.*, 1988, **93**, 1407.
- 9 R. A. Rasmussen and M. A. K. Khalil, *J. Geophys. Res.*, 1988, **93**, 1417.
- 10 Y. Yokouchi and A. Yoshinari, *J. Geophys. Res.*, 1988, **93**, 3751.
- 11 M. E. Jenkin and R. A. Cox, *J. Phys. Chem.*, 1991, **95**, 3229.
- 12 T. P. Murrells, M. E. Jenkin, S. J. Shalliker and G. D. Hayman, *J. Chem. Soc., Faraday Trans.*, 1991, **87**, 2351.
- 13 H. E. Van den Bergh and A. B. Callear, *Trans. Faraday Soc.*, 1970, **66**, 2681.
- 14 J. M. Tulloch, M. T. Macpherson, C. A. Morgan and M. J. Pilling, *J. Phys. Chem.*, 1982, **86**, 3812.
- 15 C. A. Morgan, M. J. Pilling, J. M. Tulloch, R. P. Ruiz and K. P. Bayes, *J. Chem. Soc., Faraday Trans. 2*, 1982, **78**, 1323.
- 16 R. A. Cox and G. D. Hayman, *Nature (London)*, 1988, **332**, 796.
- 17 A. R. Curtis and W. P. Sweetenham, AERE Report RM. 12805, 1987.
- 18 M. E. Jenkin, R. A. Cox, A. Mellouki, G. Le Bras and G. Poulet, *J. Phys. Chem.*, 1990, **94**, 2927.
- 19 E. P. Gardiner, P. D. Sperry and J. G. Calvert, *J. Phys. Chem.*, 1987, **91**, 1922.
- 20 (a) J. Y. Park, M. C. Heaven and D. Gutman, *Chem. Phys. Lett.*, 1984, **104**, 469; (b) I. R. Slagle, J. Y. Park, M. C. Heaven and D. Gutman, *J. Am. Chem. Soc.*, 1984, **106**, 4536.
- 21 R. Atkinson, D. L. Baulch, R. A. Cox, R. F. Hampson, J. A. Kerr and J. Troe, *J. Phys. Chem. Ref. Data*, 1989, **18**, 881.
- 22 *CRC Handbook of Bimolecular and Termolecular Gas Reactions*, ed. J. A. Kerr and S. J. Moss, CRC Press, Boca Raton, 1981.
- 23 H. Adachi and N. Basco, *Int. J. Chem. Kinet.*, 1982, **14**, 1125.
- 24 T. J. Wallington, J. M. Andino and S. M. Japar, *Chem. Phys. Lett.*, 1990, **165**, 189.
- 25 G. Yarwood, N. Peng and H. Niki, presented at XIX Informal Conference on Photochemistry, Ann Arbor, Michigan 24-29 June, 1990.

- 26 P. Dagaut, T. J. Wallington and M. J. Kurylo, *Chem. Phys. Lett.*, 1988, **146**, 589.
- 27 J. N. Crowley and G. K. Moortgat, *J. Chem. Soc., Faraday Trans.*, 1992, **88**, 2437.
- 28 G. K. Moortgat, R. A. Cox, G. Schuster, J. P. Burrows and G. S. Tyndall, *J. Chem. Soc., Faraday Trans. 2*, 1989, **85**, 809.
- 29 C. L. Gu, C. M. Rynard, D. G. Hendry and T. Mill, *Environ. Sci. Technol.*, 1985, **19**, 151.
- 30 R. Atkinson, S. M. Aschmann, E. C. Tuazon, J. Arey and B. Zelinska, *Int. J. Chem. Kinet.*, 1989, **21**, 593.
- 31 E. C. Tuazon and R. Atkinson, *Int. J. Chem. Kinet.*, 1990, **22**, 1221.
- 32 S. E. Paulson, R. C. Flagan and J. H. Seinfeld, *Int. J. Chem. Kinet.*, 1992, **24**, 79.
- 33 K. H. Becker, H. Geiger and P. Wiesen, *Chem. Phys. Lett.*, 1991, **184**, 256.
- 34 R. Atkinson, *J. Phys. Chem. Ref. Data*, 1989, Monograph 1.
- 35 (a) M. E. Jenkin, AEA Environment and Energy Report, AEA-EE-0405, 1992; (b) I. Barnes, B. Bonsang, T. Brauers, P. Carlier, R. A. Cox, H. P. Dorn, M. E. Jenkin, G. Le Bras and U. Platt, CEC Air Pollution Research Report 35, 1991.
- 36 S. E. Paulson, R. C. Flagan and J. H. Seinfeld, *Int. J. Chem. Kinet.*, 1992, **24**, 103.
- 37 R. Atkinson, S. M. Aschmann, J. Arey and B. Shorees, *J. Geophys. Res.*, 1992, **97**, 6065.
- 38 R. P. Wayne, I. Barnes, P. Biggs, J. P. Burrows, C. E. Canosa-Mas, J. Hjorth, G. Le Bras, G. K. Moortgat, D. Perner, G. Poulet, G. Restelli and H. Sidebottom, *Atmos. Environ. A*, 1991, **25**, 1.
- 39 A. M. Winer, R. Atkinson and J. N. Pitts, *Science*, 1984, **224**, 156.

Paper 2/04041G; Received July 28th, 1992